
Spectral Augmentations for Graph Contrastive Learning

Amur Ghose
Huawei

Yingxue Zhang
Huawei

Jianye Hao
Huawei, Tianjin University

Mark Coates
McGill

Abstract

Contrastive learning has emerged as a premier method for learning representations with or without supervision. Recent studies have shown its utility in graph representation learning for pre-training. Despite successes, the understanding of how to design effective graph augmentations that can capture structural properties common to many different types of downstream graphs remains incomplete. We propose a set of well-motivated graph transformation operations derived via graph spectral analysis to provide a bank of candidates when constructing augmentations for a graph contrastive objective, enabling contrastive learning to capture useful structural representation from pre-training graph datasets. We first present a spectral graph cropping augmentation that involves filtering nodes by applying thresholds to the eigenvalues of the leading Laplacian eigenvectors. Our second novel augmentation reorders the graph frequency components in a structural Laplacian-derived position graph embedding. Further, we introduce a method that leads to improved views of local subgraphs by performing alignment via global random walk embeddings. Our experimental results indicate consistent improvements in out-of-domain graph data transfer compared to state-of-the-art graph contrastive learning methods, shedding light on how to design a graph learner that is able to learn structural properties common to diverse graph types.

1 Introduction

Representation learning is of perennial importance, with contrastive learning being a recent prominent technique. Taking images as an example, under this framework, a set

of transformations is applied to image samples, without changing the represented object or its label. Candidate transformations include cropping, resizing, Gaussian blur, and color distortion. These transformations are termed *augmentations* (Chen et al., 2020b; Grill et al., 2020). A pair of augmentations from the same sample are termed *positive pairs*. During training, their representations are pulled together (Khosla et al., 2020). In parallel, the representations from *negative pairs*, consisting of augmentations from different samples, are pushed apart. The contrastive objective encourages representations that are invariant to distortions but capture useful features. This constructs general representations, even without labels, that are usable downstream.

Recently, self-supervision has been employed to support the training process for graph neural networks (GNNs). Several approaches (e.g., Deep Graph Infomax (DGI) (Velickovic et al., 2019), InfoGCL (Xu et al., 2021)) rely on mutual information maximization or information bottlenecking between pairs of positive views. Other GNN pre-training strategies construct objectives or views that rely heavily on domain-specific features (Hu et al., 2020b,c). This inhibits their ability to generalize to other application domains. Some recent graph contrastive learning strategies such as GCC (Qiu et al., 2020) and GraphCL (You et al., 2020) can more readily transfer knowledge to out-of-domain graph domains, because they derive embeddings based solely on local graph structure, avoiding possibly unshared attributes entirely. However, these approaches employ heuristic augmentations such as random walk with restart and edge-drop, which are not designed to preserve graph properties and might lead to unexpected changes in structural semantics (Lee et al., 2022). There is a lack of diverse and effective graph transformation operations to generate augmentations. We aim to fill this gap with a set of well-motivated graph transformation operations derived via graph spectral analysis to provide a bank of candidates when constructing augmentations for a graph contrastive objective. This allows the graph encoder to learn structural properties that are common for graph data spanning multiple graphs and domains.

Contributions. We introduce three novel methods: (i) *spectral graph cropping*, (ii) *graph frequency component reordering*, both being graph data augmentations, and a post-processing step termed (iii) *local-global embedding align-*

Table 1: Properties of different approaches to graph contrastive (unsupervised) learning. * indicates that the method was not originally designed for pre-training, but can be trivially adapted to it. **See Appendix 1 for a more complete description with relevant references.**

Approaches	Goal is pre-training or transfer	No requirement for features	Domain transfer	Shareable graph encoder
Category 1 (DGI, InfoGraph, MVGRL, DGCL, InfoGCL, AFGRL)	✗	✗	✗	✗
Category 2 (GPT-GNN, Strategies for pre-training GNNs)	✓	✗	✗	✓
Category 3 (Deepwalk, LINE, node2vec)	✗	✓	✓	✗
Category 4 (struc2vec, graph2vec, DGK, Graphwave, InfiniteWalk)	✗	✓	✓	✗
Category 5 (GraphCL, CuCo*, GCC, BYOV, GRACE*, GCA*, Ours)	✓	✓	✓	✓

ment. We also propose a strategy to select from candidate augmentations, termed *post augmentation filtering*. *First*, we define a graph transformation that removes nodes based on the graph Laplacian eigenvectors. This generalizes the image crop augmentation. *Second*, we introduce an augmentation that reorders graph frequency components in a structural Laplacian-derived position embedding. We motivate this by showing its equivalence to seeking alternative *diffusion* matrices instead of the Laplacian for factorization. This resembles image color channel manipulation. *Third*, we introduce the approach of aligning local structural positional embeddings with a global embedding view to better capture structural properties that are common for graph data. Taken together, we improve state-of-the-art methods for contrastive learning on graphs for out-of-domain graph data transfer. We term our overall suite of augmentations **SGCL (Spectral Graph Contrastive Learning)**.

2 Related Work

Graph contrastive methods. Table 1 divides existing work into five categories. *Category 1* methods rely on mutual information maximization or bottlenecking. *Category 2* methods require that pre-train and downstream task graphs come from the same domain. *Category 3* includes random walk based embedding methods and *Category 4* includes structural similarity-based methods. These methods do not provide shareable parameters (You et al., 2020). *Category 5 (our setting)*: These methods explicitly target pre-training or transfer. Two of the more closely related approaches are Graph Contrastive Coding (GCC) (Qiu et al., 2020) and GraphCL (You et al., 2020). In GCC, the core augmentation is random walk with return (Tong et al., 2006) and Laplacian positional encoding is used to improve out-of-domain generalization. GraphCL (You et al., 2020) expands this augmentation suite by including node dropping, edge perturbations, and attribute masking. Other methods in Category 5 construct adaptive/learnable contrastive views (Zhu et al., 2021; Chu et al., 2021; You et al., 2022; Lee et al., 2022). Please see Appendix 1 for more detailed discussion.

Graph structural augmentations. We focus on the most general, adaptable and transferable *structure-only* scenario — learning a GNN encoder using a large scale pre-training

dataset with solely structural data and no attributes or labels. While not all methods in category 5 address this setting, they can be adapted to run in such conditions by removing domain or attribute-reliant steps. The graph augmentation strategy plays a key role in the success of graph contrastive learning (Qiu et al., 2020; You et al., 2020; Li et al., 2021; Sun et al., 2019; Hassani and Khasahmadi, 2020; Xu et al., 2021) and is a natural target as our area of focus. Commonly-used graph augmentations include: 1) attribute dropping or masking (You et al., 2020; Hu et al., 2020c); 2) random edge/node dropping (Li et al., 2021; Xu et al., 2021; Zhu et al., 2020, 2021); 3) graph diffusion (Hassani and Khasahmadi, 2020) and 4) random walks around a center node (Tong et al., 2006; Qiu et al., 2020). Additionally, there is an augmentation called GraphCrop (Wang et al., 2020), which uses a node-centric strategy to crop a contiguous subgraph from the original graph while maintaining its connectivity; this is different from the spectral graph cropping we propose. Existing structure augmentation strategies are not tailored to any special graph properties and might unexpectedly change the semantics (Lee et al., 2022).

Positioning our work. Encoding human-interpretable structural patterns such as degree, triangle count, and graph motifs, is key to successful architectures such as GIN (Xu et al., 2019) or DiffPool (Ying et al., 2018) and these patterns control the quality of out-of distribution transfer (Yehudai et al., 2021) for graph tasks, which naturally relates to the pre-train framework where the downstream dataset may differ in distribution from the pre-train corpus. We seek a GNN which learns to capture structural properties common to diverse types of downstream graphs.

These commonly used structural patterns (e.g., degree, triangle count) are handcrafted. It is preferable to learn these features instead of defining them by fiat. Our goal is to create an unsupervised method that learns functions of the graph structure alone, which can freely transfer downstream to any task. The use of spectral features to learn these structural embeddings is a natural choice; spectral features such as the second eigenvalue or the spectral gap relate strongly to purely structural features such as the number of clusters in a graph, the number of connected components, and the d-regularity (Spielman, 2007). Methods based on spectral eigendecomposition such as Laplacian embeddings are ubiq-

uitous, and even random-walk based embeddings such as LINE (Tang et al., 2015) are simply eigendecompositions of transformed adjacency matrices. Instead of handcrafting degree-like features, we strive to construct a learning process that allows the GNN to learn, in an unsupervised fashion, useful structural motifs. By founding the process on the spectrum of the graph, learning can move freely between the combinatorial, discrete domain of the nodes and the algebraic domain of embeddings.

Such structural features are required for the **structure-only** case, where we have large, unlabeled, pre-train graphs, and no guarantee that any attributes are shared with the downstream task. This is the most challenging setting in graph pre-training. In such a setting, it is only structural patterns that can be learned from the corpus and potentially transferred and employed in the downstream phase.

3 Graph Contrastive Learning

We consider a setting where we have a set of graphs $\mathcal{G} = \{G_t\}$ available for pre-training using contrastive learning. If we are addressing graph-level downstream tasks, then we work directly with the G_t . However, if the task is focused on nodes (e.g., node classification), then we associate with each node $i \in G_t$ a subgraph G_i , constructed as the r -ego subnetwork around i in G_t , defined as

$$G_i \triangleq G_t[\{v \in G_t : d(i, v) \leq r\}], \quad (1)$$

where $d(u, v)$ is the shortest path distance between nodes u and v and $G[S]$ denotes the subgraph induced from G by the subset of vertices S . During pre-training there are no labels, but in a fine-tuning phase when labels may be available, a subgraph G_i inherits any label associated with node i . Thus, node classification is treated as graph classification, finding the label of G_i . This processing step allows us to treat node and graph classification tasks in a common framework.

Our goal is to construct an encoder parametrized by θ , denoted \mathcal{E}_θ , such that for a set of instances $G_i \in \mathcal{G}$, the output $\mathcal{E}_\theta(G_i)$ captures the essential information about G_i required for downstream tasks. We employ instance discrimination as a contrastive learning objective and minimize (Gutmann and Hyvärinen, 2010, 2012; Hjelm et al., 2018):

$$-\log \frac{\exp\langle \mathcal{E}_\theta(G'+), \mathcal{E}_{\theta'}(G+) \rangle}{\langle \mathcal{E}_\theta(G'+), \mathcal{E}_{\theta'}(G+) \rangle + \sum_{j=1}^r \langle \mathcal{E}_\theta(G'+), \mathcal{E}_{\theta'}(G_j-) \rangle}. \quad (2)$$

Here, $G+$, $G'+$ may be any augmented version of G , and one of them can be G itself. There is an additional sum in the denominator, denoting the number of negative instances.

For the encoder, we construct *structure positional embeddings* generalizable to unseen graphs. Let G_i have N nodes, adjacency matrix \mathbf{A}_i , diagonal degree matrix \mathbf{D}_i . The normalized Laplacian of G_i is \mathbf{L}_i , which is eigendecomposed:

$$\mathbf{L}_i = \mathbf{I} - \mathbf{D}_i^{-1/2} \mathbf{A}_i \mathbf{D}_i^{-1/2}, \quad \mathbf{U}_i \mathbf{\Lambda}_i \mathbf{U}_i^T = \mathbf{L}_i. \quad (3)$$

With the $\mathbf{\Lambda}_i$ (eigenvalues) sorted in ascending order of magnitude, the first k columns of \mathbf{U}_i yield the k -dimensional positional embedding, \mathbf{X}_i , of shape $N \times k$. The pair (G_i, \mathbf{X}_i) then serves as input to a GNN graph encoder (in our case GIN (Xu et al., 2019)), which creates a corresponding hidden vector \mathbf{H}_i of shape $N \times h$, where h is the dimensionality of the final GNN layer. Each row corresponds to a vertex $v \in G_i$. A readout function (Gilmer et al., 2017; Xu et al., 2019), which can be a simple permutation invariant function such as summation, or a more complex graph-level pooling function, takes the hidden states over $v \in G_i$ and creates an h -dimensional graph representation \mathbf{r}_i . A view of G_i can be created by conducting an independent random walk (with return) from node i , and collecting all the nodes visited in the walk to form G'_i . The random walk captures the local structure around i in G_i while perturbing it, and is inherently *structural*. A random walk originating from another node $j \in G_j, j \neq i$ leads to a negative example G_j- .

4 Spectral Graph Contrastive Augmentation Framework

In this work, we introduce two novel graph data augmentation strategies: *graph cropping* and *reordering of graph frequency components*. We also propose two important quality-enhancing mechanisms. The first, which we call *augmentation filtering*, selects among candidate augmentations based on their representation similarity. The second, called *local-global embedding view alignment*, aligns the representations of the nodes that are shared between augmentations. We add the masking attribute augmentation (Hu et al., 2020b) which randomly replaces embeddings with zeros to form our overall flow of operations for augmentation construction, as depicted in Figure 1. The first two mandatory steps are ego-net formation and random walk. Subsequent steps may occur (with probabilities as $p_{filter}, p_{crop}, p_{align}, p_{mask}, p_{reorder}$) or may not. Two of the steps — mask and reorder — are mutually exclusive. For more detail, see Appendix 4.4. In the remainder of the section, we provide a detailed description of the core novel elements in the augmentation construction procedure: (i) spectral **cropping**; (ii) frequency component **reordering**; (iii) **similar** filtering; and (iv) embedding **alignment**. We aim to be as general as possible and graphs are a general class of data - images, for instance, may be represented as grid graphs. Our general graph augmentations such as “cropping” reduce to successful augmentations in the image domain, lending them credence, as a general method should excel in all sub-classes it contains.

4.1 Graph cropping using eigenvectors.

The image cropping augmentation is extremely effective (Chen et al., 2020b; Grill et al., 2020). It trims pixels along the (x, y) axes. There is no obvious way to extend this

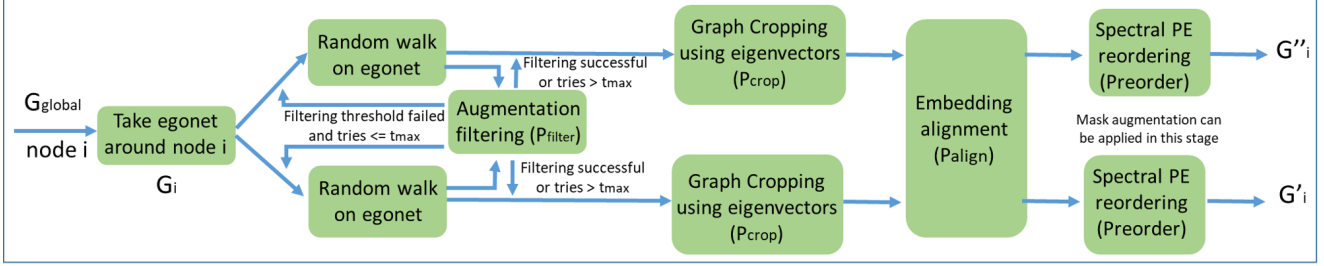


Figure 1: Overall framework of SGCL. A box denotes an augmentation that may change the graph with probability denoted or leave it unchanged. Final two augmentations are mutually exclusive. t_{max} denotes the maximum number of tries permitted to the filtering step.

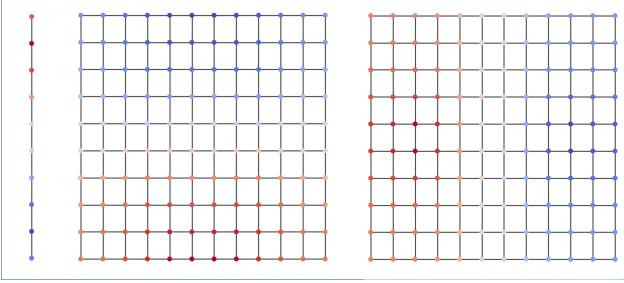


Figure 2: Fiedler eigenvector induced values on a line graph via λ_2 , which change monotonically along the graph, translate into eigenvector values for the grid graph with λ_2, λ_3 .

operation to general (non-grid) graphs. We now introduce a graph cropping augmentation that removes nodes using the eigenvectors corresponding to the two smallest non-zero eigenvalues of the graph Laplacian L_i . When eigenvalues are non-decreasingly sorted, the second eigenvector (corresponding to the lowest nonzero eigenvalue) provides a well-known method to partition the graph — the *Fiedler cut*. We use the eigenvectors corresponding to the first two nonzero eigenvalues, λ_2 and λ_3 . Let $\mathbf{x}(v)$ denote the value assigned to node v in the second eigenvector, and similarly $\mathbf{y}(v)$ with the third eigenvector corresponding to λ_3 . We define the spectral **crop** augmentation as: $G_i[x_{\min}, x_{\max}, y_{\min}, y_{\max}]$ (a cropped view) being the set of vertices $v \in G_i$ satisfying $x_{\min} \leq \mathbf{x}(v) \leq x_{\max}$ and $y_{\min} \leq \mathbf{y}(v) \leq y_{\max}$.

Link to image cropping: We claim that the proposed graph cropping generalizes image cropping. Let us view the values of the eigenvector corresponding to λ_2 on a *line graph* (Figure 2). If we set a threshold t , and retain only the nodes with eigenvector values below (above) the threshold, we recover a contiguous horizontal segment of the graph. Thus, the eigenvector for λ_2 corresponds to variation along an axis (Ortega et al., 2018; Chung and Graham, 1997; Davies et al., 2000), much like the x or y axis in an image.

We consider now a *product graph*. A product of two graphs A, B with vertex sets (v_A, v_B) and edge sets (e_A, e_B) is a graph $A.B$ where each $v \in A.B$ can be identified with an ordered pair $(i, j), i \in v_A, j \in v_B$. Two nodes corresponding

to $(i, j), (i', j')$ in $A.B$ have an edge between them if and only if either $i' = i, (j, j') \in v_B$ or $(i, i') \in v_A, j = j'$. The product of two line graphs of length M, N respectively is representable as a planar rectangular grid of lengths M, N .

Denote by P_n the path-graph on n vertices, which has $n-1$ edges of form $(i, i+1)$ for $i = 1, \dots, n-1$. This corresponds to the line graph. Denote by $G_{a,b}$ the rectangular grid graph formed by the product $P_a.P_b$. Structurally, this graph represents an image with dimensions $a \times b$. The eigenvectors of the (un-normalized) Laplacian of P_n , for $n > k \geq 0$, are of the form: $\mathbf{x}_k(u) = \cos(\pi k u / n - \pi k / 2n)$, with eigenvalues $2 - 2 \cos(\pi k / n)$. Clearly, $k = 0$ yields the constant eigenvector. The first nonzero eigenvalue corresponds to $k = 1$, where the eigenvector completes one “period” (with respect to the cosine’s argument) over the path, and it is this pattern that is shown in Figure 2.

The following properties are well-known for the spectrum of product graphs (Brouwer and Haemers, 2011). Each eigenvalue is of the form $\lambda_i + \lambda_j$, where λ_i is from the spectrum of P_a and λ_j from P_b . Further, the corresponding eigenvector $\mathbf{v}_{i,j}$ satisfies $\mathbf{v}_{i,j}(u, v) = \mathbf{x}_i(u)\mathbf{y}_j(v)$, where $\mathbf{x}_i, \mathbf{y}_j$ denote the eigenvectors from the respective path graphs. This means, for the spectra of $G_{a,b}$, that the lowest eigenvalue of the Laplacian corresponds to the constant eigenvector, and the second lowest eigenvalue corresponds to the constant eigenvector along one axis (path) and $\cos(\pi u / n - \pi / 2n)$ along another. The variation is along the larger axis, i.e., along a , because the $2 - 2 \cos(\pi k / n)$ term is smaller. This implies that for $G_{a,b}, 2b > a > b$, λ_2, λ_3 correspond to eigenvectors that recover axes in the grid graph (Figure 2).

4.2 Frequency-based positional embedding reordering

Images have multi-channel data, derived from the RGB encoding. The channels correspond to different frequencies of the visible spectrum. The successful color reordering augmentation for images (Chen et al., 2020b) thus corresponds to a permutation of frequency components. This motivates us to introduce a novel augmentation that is derived by reordering the graph frequency components in a structural position embedding. A structural position embed-

ding can be obtained by factorization of the graph Laplacian. The Laplacian eigendecomposition corresponds to a frequency-based decomposition of signals defined on the graph (Von Luxburg, 2007a; Chung and Graham, 1997). We thus consider augmentations that permute, i.e., *reorder*, the columns of the structural positional embedding \mathbf{X}_i .

However, *arbitrary* permutations do not lead to good augmentations. In deriving a position embedding, the normalized Laplacian \mathbf{L}_i is not the only valid choice of matrix to factorize. Qiu et al. (2018) show that popular random walk embedding methods arise from the eigendecompositions of:

$$\log\left(\sum_{j=1}^r (\mathbf{I} - \mathbf{L}_i)^r\right) \mathbf{D}_i^{-1} = \log\left(\mathbf{U}_i \left(\sum_{j=1}^r (\mathbf{I} - \mathbf{A}_i)^r\right) \mathbf{U}_i^T\right) \mathbf{D}_i^{-1}. \quad (4)$$

We have excluded negative sampling and graph volume terms for clarity. We observe that $\sum_{j=1}^r (\mathbf{I} - \mathbf{L}_i)^r$ replaces $(\mathbf{I} - \mathbf{L}_i)$ in the spectral decomposition. Just as the adjacency matrix \mathbf{A}_i encodes the first order proximity (edges), \mathbf{A}_i^2 encodes second order connectivity, \mathbf{A}_i^3 third order and so on. Using larger values of r in equation 4 thus integrates higher order information in the embedding. The sought-after eigenvectors in \mathbf{X} are the columns in \mathbf{U} corresponding to the top k values of $\sum_{j=1}^r (1 - \lambda)^j$. There is no need to repeat the eigendecomposition to obtain a new embedding. The higher-order embedding is obtained by *reordering* the eigenvectors (in descending order of $\sum_{j=1}^r (1 - \lambda_w)^j$).

This motivates our proposed reordering augmentation and identifies suitable permutation matrices. Rather than permute all of the eigenvectors in the eigendecomposition, for computational efficiency, we first extract the k eigenvectors with the highest corresponding eigenvalues in the first order positional embedding derived using $(\mathbf{I} - \mathbf{L}_i)$. The reordering augmentation only permutes those k eigenvectors. The augmentation thus forms $\mathbf{X}_i \mathbf{P}_r$ where \mathbf{P}_r is a permutation matrix of shape $k \times k$. The permutation matrix \mathbf{P}_r sorts eigenvectors with respect to the values $\sum_{j=1}^r (1 - \lambda_w)^j$. We randomize the permutation matrix generation step by sampling an integer uniformly in the range $[1, r_{max}]$ to serve as r and apply the permutation to produce the view G'_i .

4.3 Embedding alignment

In this subsection and the next, we present two quality enhancing mechanisms that are incorporated in our spectral augmentation generation process and lead to superior augmentations. Both use auxiliary global structure information.

Consider two vertices v and v' in the same graph G_t . Methods such as Node2vec (Grover and Leskovec, 2016), LINE (Tang et al., 2015), & DeepWalk (Perozzi et al., 2014) operate on G_t outputting an embedding matrix \mathbf{E}_t . The row corresponding to vertex v provides a node embedding e_v .

Node embedding alignment allows comparing embeddings between disconnected graphs G_1, G_2 utilizing the structural

connections in each graph (Singh et al., 2007; Chen et al., 2020c; Heimann et al., 2018; Grave et al., 2019). Consider two views G'_i, G''_i and a node v_i such that $v_i \in G'_i, v_i \in G''_i$. Given the embeddings $\mathbf{X}'_i, \mathbf{X}''_i$ for G'_i, G''_i , ignoring permutation terms, alignment seeks to find an orthogonal matrix \mathbf{Q} satisfying $\mathbf{X}''_i \mathbf{Q} \approx \mathbf{X}'_i$. If the embedding is computed via eigendecomposition of $\mathbf{L}'_i, \mathbf{L}''_i$, the final structural node embeddings (rows corresponding to v_i in $\mathbf{X}'_i, \mathbf{X}''_i$) for v_i may differ. To correct this, we align the structural features $\mathbf{X}'_i, \mathbf{X}''_i$, using the global matrix \mathbf{E}_t as a bridge.

Specifically, let $N_{G'_i}$ be the sub-matrix of \mathbf{E}_t obtained by collecting all rows j such that $v_j \in G_i$. Define $N_{G''_i}$ similarly. We find an orthogonal matrix $\mathbf{Q}^* = \min_{\mathbf{Q}} \|\mathbf{X}'_i \mathbf{Q} - N_{G'_i}\|^2$. The solution is $\mathbf{A}\mathbf{C}^T$, where $\mathbf{A}\mathbf{B}\mathbf{C}^T$ is the singular value decomposition (SVD) of $(\mathbf{X}'_i)^T N_{G'_i}$ (Heimann et al., 2018; Chen et al., 2020c). Similarly, we compute \mathbf{Q}^{**} for G''_i . We consider the resulting matrices $\mathbf{X}'_i \mathbf{Q}^* \approx N_{G'_i}$ and $\mathbf{X}''_i \mathbf{Q}^{**} \approx N_{G''_i}$. Since $N_{G'_i}, N_{G''_i}$ are both derived from \mathbf{E}_t , the rows (embeddings) corresponding to a common node are the same. We can thus derive improved augmentations by reducing the undesirable disparity induced by misalignment and replacing $\mathbf{X}'_i, \mathbf{X}''_i$ with their aligned counterparts $\mathbf{X}'_i \mathbf{Q}^*, \mathbf{X}''_i \mathbf{Q}^{**}$, terming this as **align**.

4.4 Augmentation filter.

Consider two views G'_i, G''_i resulting from random walks from a node a_i of which G_i is the ego-network in G_t . Let $\mathbf{E}_{G'_i} = \sum_{v_z \in G'_i} \mathbf{e}_z$. We can measure the similarity of the views as $\langle \mathbf{E}_{G'_i}, \mathbf{E}_{G''_i} \rangle$. To enforce **similar filtering** of views, we accept the views if they are similar to avoid potential noisy augmentations: $\frac{\langle \mathbf{E}_{G'_i}, \mathbf{E}_{G''_i} \rangle}{\|\mathbf{E}_{G'_i}\| \|\mathbf{E}_{G''_i}\|} > 1 - c$, for some constant $0 \leq c \leq 1$. (For choice of c , see appendix 4.3.) We couple this filtering step with the random walk to accept candidates (Figure 1). Please note that applying similarity filtering empirically works much better than the other possible alternative, diverse filtering. We present the ablation study in appendix section 4.5.

4.5 Theoretical analysis.

We conduct a theoretical analysis of the spectral crop augmentation. In the Appendix, we extend this to a variant of the similar filtering operation. We investigate a simple case of the two-component stochastic block model (SBM) with $2N$ nodes divided equally between classes 0, 1. These results are also extensible to certain multi-component SBMs. Let the edge probabilities be p for edges between nodes of class 0, q for edges between nodes of class 1, and z for edges between nodes of different classes. We assume that $p > q > z > 0$.

Denote by G a random graph from this SBM. We define the class, $Y(G)$, to be the majority of the classes of its nodes, with $Y(v)$ being the class of a node v . Let $E_{d,v}(G)$ denote

Table 2: Datasets for pre-training, sorted by number of vertices. Bolded dataset indicates use for ablation.

Dataset	DBLP (SNAP)	Academia	DBLP (NetRep)	IMDB	Facebook	LiveJournal
Nodes	317,080	137,969	540,486	896,305	3,097,165	4,843,953
Edges	2,099,732	739,384	30,491,458	7,564,894	47,334,788	85,691,368

the ego-network of v up to distance d in G . Let $C_\epsilon(v)$ be the cropped local neighbourhood around node v defined as $\{v' : \|\lambda(v') - \lambda(v)\| \leq \epsilon\}$ where $\lambda(v) = [\lambda_2(v), \lambda_3(v)]$, with λ_j as the j -th eigenvector (sorted in ascending order by eigenvalue) of the Laplacian of G . In the Appendix, we prove the following result:

Theorem 1 *Let node v be chosen uniformly at random from G , a $2N$ -node graph generated according to the SBM described above. With probability $\geq 1 - f(N)$ for a function $f(N) \rightarrow 0$ as $N \rightarrow \infty$, $\exists \epsilon \in \mathbb{R}^+$, $k_{max} \in \mathbb{N}$ such that :*

$$\forall k \in \mathbb{N} \leq k_{max}, Y(E_{k,v}(G)) = Y(C_\epsilon(v)) = Y(v) \quad (5)$$

This theorem states that for the SBM, both a view generated by the ego-network and a view generated by the crop augmentation acquire, with high probability as the number of nodes grows, graph class labels that coincide with the class of the centre node. This supports the validity of the crop augmentation — it constructs a valid “positive” view.

We further analyze global structural embeddings and similar/diverse filtering, and specify $f(N)$, in Appendix 10.

The proof of Theorem 1 relies on the Davis-Kahan theorem. Let $\mathbf{A}, \mathbf{H} \in \mathbb{R}^{N \times N}$, $\mathbf{A} = \mathbf{A}^T$, $\mathbf{H} = \mathbf{H}^T$ with $\mu_1 \geq \mu_2 \geq \dots \mu_N$ the eigenvalues of \mathbf{A} , $\mathbf{v}_1, \mathbf{v}_2, \dots, \mathbf{v}_N$ the corresponding eigenvectors of \mathbf{A} , and $\mathbf{v}'_1, \mathbf{v}'_2, \dots, \mathbf{v}'_N$ those of $\mathbf{A} + \mathbf{H}$. By the Davis-Kahan theorem (Demmel, 1997) (Theorem 5.4), if the angle between $\mathbf{v}_i, \mathbf{v}'_i$ is θ_i , then, with $\|\mathbf{H}\|_{op}$ as the max eigenvalue by magnitude of \mathbf{H}

$$\sin(2\theta_i) \leq \frac{2\|\mathbf{H}\|_{op}}{N \times \min_{j \neq i} |\mu_i - \mu_j|} \quad (6)$$

In our setting, we consider $\mathbf{A} + \mathbf{H}$ to be the adjacency matrix of the observed graph, which is corrupted by some noise \mathbf{H} applied to a “true” adjacency matrix \mathbf{A} . The angle θ_i measures how this noise \mathbf{H} impacts the eigenvectors, which are used in forming Laplacian embeddings and also in the cropping step. Consider θ_2 , the angular error in the second eigenvector. For a normalized adjacency matrix, such that $\mu_1 = 1$, this error scales as $\frac{1}{\min(\mu_2 - \mu_3, \mu_1 - \mu_2)}$. We can anticipate that the error is larger as μ_2 becomes larger ($\mu_1 - \mu_2$ falls) or smaller ($\mu_2 - \mu_3$ falls). The error affects the quality of the crop augmentation and the quality of generated embeddings. In Section 5.2, we explore the effectiveness of the augmentations as we split datasets by their spectral properties (by an estimate of μ_2). As expected, we observe that the crop augmentation is less effective for graphs with large or small (estimated) μ_2 .

5 Experiments

Datasets. The datasets for pretraining are summarized in Table 2. They are relatively large, with the largest graph having ~ 4.8 million nodes and ~ 85 million edges. Key statistics of the downstream datasets are summarized in the individual result tables. Our primary node-level datasets are US-Airport (Ribeiro et al., 2017) and H-index (Zhang et al., 2019a) while our graph datasets derive from (Yanardag and Vishwanathan, 2015) as collated in (Qiu et al., 2020). Node-level tasks are at all times converted to graph-level tasks by forming an ego-graph around each node, as described in Section 3. We conduct similarity search tasks over the academic graphs of data mining conferences following (Zhang et al., 2019a). Full dataset details are in Appendix section 4.

Training scheme. We use two representative contrastive learning training schemes for the graph encoder via minibatch-level contrasting (E2E) and MoCo (He et al., 2020) (Momentum-Contrasting). In all experiment tables, we present results where the encoder only trains on pre-train graphs and never sees target domain graphs. In Appendix 4, we provide an additional setting where we fully fine-tune all parameters with the target domain graph after pre-training. We construct all graph encoders (ours and other baselines) as a 5 layer GIN (Xu et al., 2019) for fair comparison.

Competing baselines. As noted in our categorization of existing methods in Table 1, the closest analogues to our approach are GraphCL (You et al., 2020) and GCC (Qiu et al., 2020) which serve as our key benchmarks. Additionally, although they are not designed for pre-training, we integrated the augmentation strategies from MVGRL (Hassani and Khasahmadi, 2020), Grace (Zhu et al., 2020), Cuco (Chu et al., 2021), and Bringing Your Own View (BYOV) (You et al., 2022) to work with the pre-train setup and datasets we use. We include additional baselines that are specifically tailored for each downstream task and require unsupervised pre-training on target domain graphs instead of our pre-train graphs. We include Struc2vec (Ribeiro et al., 2017), ProNE (Zhang et al., 2019b), and GraphWave (Donnat et al., 2018) as baselines for the node classification task. For the graph classification task, we include Deep Graph Kernel (DGK) (Yanardag and Vishwanathan, 2015), graph2vec (Narayanan et al., 2017), and InfoGraph (Sun et al., 2019) as baselines. For the top-k similarity search method, two specialized methods are included: Panther (Zhang et al., 2015) and RoIX (Henderson et al., 2012). All results for GCC are copied from (Qiu et al., 2020). For GraphCL (You et al., 2020), we re-implemented the described augmentations to work with the pre-training

set up and datasets we use. We also add two strong recent benchmarks, namely InfoGCL (Xu et al., 2021) and GCA (You et al., 2021). Some strong baselines such as G-MIXUP (Han et al., 2022) were excluded because they require labels during the pre-training phase.

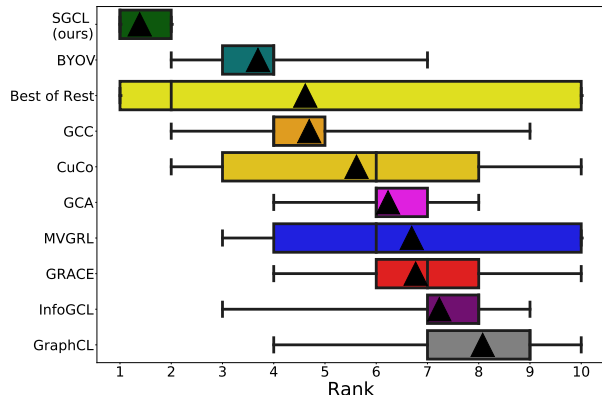


Figure 3: A rank test across 10 datasets including node and graph level classification and similarity search.



Figure 4: Heatmap indicating the effectiveness of each augmentation, pairwise, on reddit-binary. Numbers are percentage improvement relative to the SOTA method GCC (Qiu et al., 2020).

Performance metrics. After pre-training, we train a regularized logistic regression model (node classification) or SVM classifier (graph classification) from the scikit-learn package on the obtained representations using the target graph data, and evaluate using $k = 10$ fold splits of the dataset labels. Following (Qiu et al., 2020), we use F-1 score (out of 100) as the metric for node classification tasks, accuracy percentages for graph classification, and HITS@10 (top 10 accuracy) at top $k = 20, 40$ for similarity search.

Experimental procedure. We carefully ensure our reported results are reproducible and accurate. We run our model 80 times with different random seeds; the seed controls the random sampler for the augmentation generation and the initialization of neural network weights. We conduct three statistical tests to compare our method with the second best baseline under both E2E and MoCo training schemes: Wilcoxon signed-rank (Woolson, 2007), Whitney-Mann (McKnight and Najab, 2010), and the t-test. Statistical significance is declared if the p-values for all tests are

less than 10^{-6} . Appendix 4 details hyperparameters, experimental choices and statistical methodologies. Standard deviations, statistical test results, and confidence intervals are provided in Appendix 5, and additional experimental results for the CIFAR-10, MNIST, and OGB datasets are presented in Appendix 6.

Table 3: Runtime comparison (seconds per mini-batch)

MVGRL PPR	MVGRL heat	GraphCL	GRACE	GCC	SGCL (Ours)
2.34	0.164	0.079	0.074	0.063	0.084

5.1 Runtime and scaling considerations

Table 3 reports running time per mini-batch (with batch size 16) for baselines and our proposed suite of augmentations. We observe a significant increase in computation cost for MVGRL (Hassani and Khasahmadi, 2020), introduced by the graph diffusion operation (Page et al., 1999; Kondor and Lafferty, 2002). The operation is more costly than the Personalized Page Rank (PPR) (Page et al., 1999) based transition matrix since it requires an inversion of the adjacency matrix. Other baselines, as well as our method, are on the same scale, with GCC being the most efficient. Additional time analysis is present in Appendix section 11.

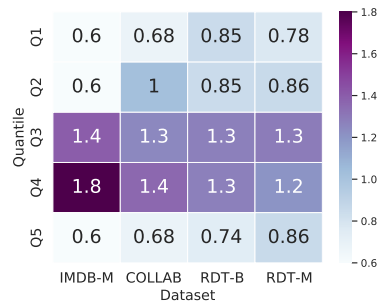


Figure 5: Heatmap indicating the effectiveness of SGCL on quintiles split by the second eigenvalue. Numbers are percentage improvement relative to the SOTA method GCC (Qiu et al., 2020)

5.2 Results and Discussion

We report the performance of our model as well as other baselines on node classification and on graph classification in Table 5.1. Top- k similarity search results are provided in Appendix 4.6. We report both the average performance across 80 trials and confidence intervals (Appendix 5) for our proposed design, GraphCL (You et al., 2020), MVGRL (Hassani and Khasahmadi, 2020), Grace (Zhu et al., 2020), Cuco (Chu et al., 2021) and BYOV (You et al., 2022). Confidence intervals indicate a span between the 5-th and 95-th percentiles, estimated by bootstrapping over splits and random seeds. For the other baselines, we copy the results reported in (Qiu et al., 2020).

Our design achieves robust improvement on both node and graph classification tasks over other baselines for the domain

Table 4: Graph (left) and node (right) classification results when the pre-trained graph encoder transfers to an out-of-domain graph. "-" indicates the model cannot produce reasonable results after 24 hours of training, as explained in (Qiu et al., 2020). Bold indicates best result; asterisk indicates statistical significant difference from next best. Appendix 5 provides standard deviations and confidence intervals.

Graph Classification											Node Classification				
Datasets	IMDB-B		IMDB-M		COLLAB		RDT-B		RDT-M		Datasets	US-Airport		H-index	
# graphs	1,000		1,500		5,000		2,000		5,000		$ V $	1,190		5,000	
# classes	2		3		3		2		5		$ E $	13,599		44,020	
Avg. # nodes	19.8		13.0		74.5		429.6		508.5		ProNE	62.3		69.1	
DGK	67.0		44.6		73.1		78.0		41.3		GraphWave	60.2		70.3	
graph2vec	71.1		50.4		-		75.8		47.9		Struc2vec	66.2		≥ 1 Day	
InfoGraph	73.0		49.7		-		82.5		53.5		Training mode	MoCo	E2E	MoCo	E2E
Training mode	MoCo	E2E	MoCo	E2E	MoCo	E2E	MoCo	E2E	MoCo	E2E	MoCo	E2E	MoCo	E2E	
GCC	72.0	71.7	49.4	49.3	78.9	74.7	89.8	87.5	53.7	52.6	GCC	65.6	64.8	75.2	78.3
GraphCL	72.2	70.9	49.3	47.9	77.2	74.1	88.7	87.2	52.9	51.8	GraphCL	62.8	63.5	74.3	76.5
GRACE	71.7	71.5	49.2	48.8	78.3	74.5	89.2	87.0	53.4	52.0	GRACE	62.6	63.3	74.5	77.0
CuCo	71.8	71.3	48.7	48.5	78.5	74.2	89.3	87.8	52.5	51.6	MVGRL	65.2	64.5	75.1	78.1
BYOV	72.3	72.0	48.5	49.2	78.4	75.1	89.5	87.9	53.6	53.0	CuCo	64.9	64.3	75.3	78.2
MVGRL	72.3	72.2	49.2	49.4	78.6	75.0	89.6	87.4	53.4	52.8	BYOV	65.3	64.7	76.0	78.1
InfoGCL	72.0	71.0	48.8	48.2	77.8	74.6	89.1	87.3	52.7	52.2	InfoGCL	63.2	64.1	75.4	77.6
GCA	72.2	71.9	49.0	48.7	78.4	74.4	88.9	87.5	53.2	52.4	GCA	64.5	64.3	75.8	78.0
SGCL	73.4*	73.0	50.0	49.8	79.7*	75.6	90.6*	88.4	54.2*	53.8	SGCL	65.9	65.3	76.7	78.9*

transfer setting. We emphasize that the graph encoders for all the baselines from *Category 5* in Table 1 are not trained on the target source dataset, whereas other baselines use this as training data (in an unsupervised fashion). Although this handicaps the domain transfer-based methods, our proposed method performs competitively or even significantly better compared to classic unsupervised learning approaches including ProNE (Zhang et al., 2019b), GraphWave (Donnat et al., 2018) and Struc2vec (Ribeiro et al., 2017) for node-level classification tasks and DGK, graph2vec and InfoGraph for graph level classification. We observe similar improvements relative to baselines for both the E2E and MoCo training schemes. These improvements are also evident for the similarity search task. The performance gains are also present when the encoder is fully fine-tuned on graphs from the downstream task, but due to space limitations, we present the results in Appendix 4.

Effectiveness of individual augmentations, processing/selection steps, and pairwise compositions. We show evaluation results (average over 80 trials) for both individual augmentations or filtering/selection steps and their pairwise compositions in Figure 4. For a clear demonstration, we select Reddit-binary as the downstream task and the smallest pre-train DBLP (SNAP) dataset. Using more pre-train datasets should result in further performance improvements. The full ablation study results are presented in Appendix 4. As noted previously (You et al., 2020), combining augmentations often improves the outcome. We report improvement relative to the SOTA method GCC (Qiu et al., 2020). Performance gains are observed for all augmentations. On average across 7 datasets, spectral crop emerges as the best augmentation of those we proposed. Appendix 4.5 reports the results of ablations against random variants of the crop and

reorder augmentations; the specific procedures we propose lead to a substantial performance improvement.

Performance variations due to spectral properties. We split the test graphs into quintiles based on their λ_2 values to explore whether the test graph spectrum impacts the performance of the proposed augmentation process. Figure 5 displays the improvements obtained for each quintile. As suggested by our theoretical analysis in Section 4.5, we see a marked elevation for the middle quintiles of λ_2 . These results support the conjecture that small or large values of λ_2 (an approximation of μ_2 in Section 4.5) adversely affect the embedding quality and the crop augmentation.

6 Conclusion

We introduce **SGCL**, a comprehensive suite of spectral augmentation methods suited to pre-training graph neural networks contrastively over large scale pre-train datasets. The proposed methods do not require labels or attributes, being reliant only on structure, and thus are applicable to a wide variety of settings. We show that our designed augmentations can aid the pre-training procedure to capture generalizable structural properties that are agnostic to downstream tasks. Our designs are not ad hoc, but are well motivated through spectral analysis of the graph and its connections to augmentations and other techniques in the domains of vision and network embedding analysis. The proposed augmentations make the graph encoder — trained by either E2E or MoCo — able to adapt to new datasets without fine-tuning. The suite outperforms the previous state-of-the-art methods with statistical significance. The observed improvements persist across multiple datasets for the three tasks of node classification, graph classification and similarity search.

References

- M. Belkin and P. Niyogi. Laplacian eigenmaps and spectral techniques for embedding and clustering. In *Proc. Advances in Neural Information Processing Systems*, 2001.
- A. E. Brouwer and W. H. Haemers. *Spectra of graphs*. Springer Science & Business Media, 2011.
- S. Chanpuriya and C. Musco. Infinitewalk: Deep network embeddings as laplacian embeddings with a nonlinearity. In *Proc. ACM SIGKDD Int. Conf. Knowledge Discovery & Data Mining*, 2020.
- M. Chen, Z. Wei, Z. Huang, B. Ding, and Y. Li. Simple and deep graph convolutional networks. In *Proc. Int. Conf. Machine Learning*, 2020a.
- T. Chen, S. Kornblith, M. Norouzi, and G. Hinton. A simple framework for contrastive learning of visual representations. In *Proc. Int. Conf. Machine Learning*, 2020b.
- X. Chen, M. Heimann, F. Vahedian, and D. Koutra. Cone-align: Consistent network alignment with proximity-preserving node embedding. In *Proc. ACM SIGKDD Int. Conf. Knowledge Discovery & Data Mining*, pages 1985–1988, 2020c.
- G. Chu, X. Wang, C. Shi, and X. Jiang. Cuco: Graph representation with curriculum contrastive learning. In *Proc. Int. Joint Conf. Artificial Intelligence*, 2021.
- F. R. Chung. *Spectral graph theory*, volume 92. American Mathematical Soc., 1997.
- F. R. Chung and F. C. Graham. *Spectral graph theory*. American Mathematical Soc., 1997.
- E. B. Davies, J. Leydold, and P. F. Stadler. Discrete nodal domain theorems. *arXiv preprint math/0009120*, 2000.
- J. W. Demmel. *Applied numerical linear algebra*. SIAM, 1997.
- C. Donnat, M. Zitnik, D. Hallac, and J. Leskovec. Learning structural node embeddings via diffusion wavelets. In *Proc. ACM SIGKDD Int. Conf. Knowledge Discovery & Data Mining*, pages 1320–1329, 2018.
- V. P. Dwivedi, C. K. Joshi, T. Laurent, Y. Bengio, and X. Bresson. Benchmarking graph neural networks. *arXiv preprint arXiv:2003.00982*, 2020.
- F. Errica, M. Podda, D. Bacciu, and A. Micheli. A fair comparison of graph neural networks for graph classification. *arXiv preprint arXiv:1912.09893*, 2020.
- M. Fiedler. Algebraic connectivity of graphs. *Czechoslovak mathematical journal*, 23(2):298–305, 1973.
- J. Gilmer, S. S. Schoenholz, P. F. Riley, O. Vinyals, and G. E. Dahl. Neural message passing for quantum chemistry. In *Proc. Int. Conf. Machine Learning*, 2017.
- E. Grave, A. Joulin, and Q. Berthet. Unsupervised alignment of embeddings with wasserstein procrustes. In *The 22nd International Conference on Artificial Intelligence and Statistics*, pages 1880–1890. PMLR, 2019.
- J.-B. Grill, F. Strub, F. Althché, C. Tallec, P. Richemond, E. Buchatskaya, C. Doersch, B. Avila Pires, Z. Guo, M. Gheshlaghi Azar, et al. Bootstrap your own latent—a new approach to self-supervised learning. In *Proc. Advances in Neural Information Processing Systems*, 2020.
- A. Grover and J. Leskovec. node2vec: Scalable feature learning for networks. In *Proc. ACM SIGKDD Int. Conf. Knowledge Discovery & Data Mining*, 2016.
- M. Gutmann and A. Hyvärinen. Noise-contrastive estimation: A new estimation principle for unnormalized statistical models. In *Proceedings of the thirteenth international conference on artificial intelligence and statistics*, pages 297–304, 2010.
- M. U. Gutmann and A. Hyvärinen. Noise-contrastive estimation of unnormalized statistical models, with applications to natural image statistics. *Journal of machine learning research*, 13(2), 2012.
- W. Hamilton, Z. Ying, and J. Leskovec. Inductive representation learning on large graphs. In *NeurIPS*, pages 1024–1034, 2017.
- X. Han, Z. Jiang, N. Liu, and X. Hu. G-mixup: Graph data augmentation for graph classification. *arXiv preprint arXiv:2202.07179*, 2022.
- K. Hassani and A. H. Khasahmadi. Contrastive multi-view representation learning on graphs. In *Proc. Int. Conf. Machine Learning*, 2020.
- K. He, H. Fan, Y. Wu, S. Xie, and R. Girshick. Momentum contrast for unsupervised visual representation learning. In *CVPR*, 2020.
- M. Heimann, H. Shen, T. Safavi, and D. Koutra. REGAL: Representation learning-based graph alignment. In *Proc. of CIKM*, 2018.
- K. Henderson, B. Gallagher, T. Eliassi-Rad, H. Tong, S. Basu, L. Akoglu, D. Koutra, C. Faloutsos, and L. Li. Rolx: structural role extraction & mining in large graphs. In *Proc. ACM SIGKDD Int. Conf. Knowledge Discovery & Data Mining*, 2012.
- R. D. Hjelm, A. Fedorov, S. Lavoie-Marchildon, K. Grewal, P. Bachman, A. Trischler, and Y. Bengio. Learning deep representations by mutual information estimation and maximization. *arXiv preprint arXiv:1808.06670*, 2018.
- Z. Hou, X. Liu, Y. Dong, C. Wang, J. Tang, et al. Graphmae: Self-supervised masked graph autoencoders. In *Proc. ACM SIG Int. Conf. Knowledge Discovery & Data Mining*, 2022.
- W. Hu, M. Fey, M. Zitnik, Y. Dong, H. Ren, B. Liu, M. Catasta, and J. Leskovec. Open graph benchmark: Datasets for machine learning on graphs. In *Proc. Advances in Neural Information Processing Systems*, volume 33, pages 22118–22133, 2020a.
- W. Hu, B. Liu, J. Gomes, M. Zitnik, P. Liang, V. Pande, and J. Leskovec. Strategies for pre-training graph neural

- networks. In *Proc. Int. Conf. Learning Representations*, 2020b.
- Z. Hu, Y. Dong, K. Wang, K.-W. Chang, and Y. Sun. Gpt-gnn: Generative pre-training of graph neural networks. In *Proc. ACM SIG Int. Conf. Knowledge Discovery & Data Mining*, pages 1857–1867, 2020c.
- N. Kahale. Eigenvalues and expansion of regular graphs. *Journal of the ACM (JACM)*, 42(5):1091–1106, 1995.
- P. Khosla, P. Teterwak, C. Wang, A. Sarna, Y. Tian, P. Isola, A. Maschinot, C. Liu, and D. Krishnan. Supervised contrastive learning. In *Proc. Advances in Neural Information Processing Systems*, 2020.
- T. N. Kipf and M. Welling. Semi-supervised classification with graph convolutional networks. In *Proc. Int. Conf. Learning Representations*, 2017.
- R. I. Kondor and J. Lafferty. Diffusion kernels on graphs and other discrete structures. In *Proc. Int. Conf. Machine Learning*, 2002.
- T. C. Kwok, L. C. Lau, Y. T. Lee, S. Oveis Gharan, and L. Trevisan. Improved cheeger’s inequality: Analysis of spectral partitioning algorithms through higher order spectral gap. In *Proceedings of the forty-fifth annual ACM symposium on Theory of computing*, pages 11–20, 2013.
- J. R. Lee, S. O. Gharan, and L. Trevisan. Multiway spectral partitioning and higher-order cheeger inequalities. *Journal of the ACM (JACM)*, 61(6):1–30, 2014.
- N. Lee, J. Lee, and C. Park. Augmentation-free self-supervised learning on graphs. In *AAAI*, 2022.
- H. Li, X. Wang, Z. Zhang, Z. Yuan, H. Li, and W. Zhu. Disentangled contrastive learning on graphs. In *Proc. Advances in Neural Information Processing Systems*, 2021.
- P. E. McKnight and J. Najab. Mann-whitney u test. *The Corsini encyclopedia of psychology*, pages 1–1, 2010.
- C. Morris, N. M. Kriege, F. Bause, K. Kersting, P. Mutzel, and M. Neumann. TUDataset: A collection of benchmark datasets for learning with graphs. *arXiv preprint arXiv:2007.08663*, 2020.
- A. Narayanan, M. Chandramohan, R. Venkatesan, L. Chen, Y. Liu, and S. Jaiswal. graph2vec: Learning distributed representations of graphs. *arXiv preprint arXiv:1707.05005*, 2017.
- A. Ortega, P. Frossard, J. Kovačević, J. M. Moura, and P. Vandergheynst. Graph signal processing: Overview, challenges, and applications. *Proceedings of the IEEE*, 106(5):808–828, 2018.
- L. Page, S. Brin, R. Motwani, and T. Winograd. The PageRank citation ranking: Bringing order to the web. Technical report, Stanford InfoLab, 1999.
- J. Palowitch, A. Tsitsulin, B. Mayer, and B. Perozzi. Graphworld: Fake graphs bring real insights for gnns. *arXiv preprint arXiv:2203.00112*, 2022.
- B. Perozzi, R. Al-Rfou, and S. Skiena. DeepWalk: Online learning of social representations. In *Proc. ACM SIGKDD Int. Conf. Knowledge Discovery & Data Mining*, 2014.
- K. K. Qin, F. D. Salim, Y. Ren, W. Shao, M. Heimann, and D. Koutra. G-crewe: Graph compression with embedding for network alignment. In *Proc. ACM SIG Int. Conf. Knowledge Discovery & Data Mining*, pages 1255–1264, 2020.
- J. Qiu, Y. Dong, H. Ma, J. Li, K. Wang, and J. Tang. Network embedding as matrix factorization: Unifying deepwalk, line, pte, and node2vec. In *WSDM ’18*, 2018.
- J. Qiu, Q. Chen, Y. Dong, J. Zhang, H. Yang, M. Ding, K. Wang, and J. Tang. Gcc: Graph contrastive coding for graph neural network pre-training. In *Proc. ACM SIGKDD Int. Conf. Knowledge Discovery & Data Mining*, 2020.
- L. F. Ribeiro, P. H. Saverese, and D. R. Figueiredo. struc2vec: Learning node representations from structural identity. In *Proc. ACM SIGKDD Int. Conf. Knowledge Discovery & Data Mining*, 2017.
- K. Rohe, S. Chatterjee, and B. Yu. Spectral clustering and the high-dimensional stochastic blockmodel. *The Annals of Statistics*, 39(4):1878–1915, 2011.
- P. Sarkar and P. J. Bickel. Role of normalization in spectral clustering for stochastic blockmodels. *The Annals of Statistics*, 43(3):962–990, 2015.
- R. Singh, J. Xu, and B. Berger. Pairwise global alignment of protein interaction networks by matching neighborhood topology. In *Annual International Conference on Research in Computational Molecular Biology*, 2007.
- D. A. Spielman. Spectral graph theory and its applications. In *48th Annual IEEE Symposium on Foundations of Computer Science (FOCS’07)*, pages 29–38. IEEE, 2007.
- D. A. Spielman and N. Srivastava. Graph sparsification by effective resistances. In *Proceedings of the fortieth annual ACM symposium on Theory of computing*, pages 563–568, 2008.
- F.-Y. Sun, J. Hoffman, V. Verma, and J. Tang. Infograph: Unsupervised and semi-supervised graph-level representation learning via mutual information maximization. In *Proc. Int. Conf. Learning Representations*, 2019.
- J. Tang, M. Qu, M. Wang, M. Zhang, J. Yan, and Q. Mei. LINE: Large-scale information network embedding. In *WWW ’15*, 2015.
- H. Tong, C. Faloutsos, and J.-Y. Pan. Fast random walk with restart and its applications. In *ICDM ’06*, pages 613–622. IEEE, 2006.
- L. Torres, K. S. Chan, and T. Eliassi-Rad. Glee: Geometric laplacian eigenmap embedding. *Journal of Complex Networks*, 8(2):cnaa007, 2020.

- P. Veličković, G. Cucurull, A. Casanova, A. Romero, P. Lio, and Y. Bengio. Graph attention networks. In *Proc. Int. Conf. Learning Representations*, 2018.
- P. Veličković, W. Fedus, W. L. Hamilton, P. Liò, Y. Bengio, and R. D. Hjelm. Deep graph infomax. In *Proc. Int. Conf. Learning Representations*, 2019.
- U. Von Luxburg. A tutorial on spectral clustering. *Statistics and computing*, 17(4):395–416, 2007a.
- U. Von Luxburg. A tutorial on spectral clustering. *Statistics and computing*, 17(4):395–416, 2007b.
- V. H. Vu. Spectral norm of random matrices. *Combinatorica*, 27(6):721–736, 2007.
- V. H. Vu. *Modern Aspects of Random Matrix Theory*, volume 72. American Mathematical Society, 2014.
- Y. Wang, W. Wang, Y. Liang, Y. Cai, and B. Hooi. Graphcrop: Subgraph cropping for graph classification. *arXiv preprint arXiv:2009.10564*, 2020.
- H. Weyl. Das asymptotische verteilungsgesetz der eigenwerte linearer partieller differentialgleichungen (mit einer anwendung auf die theorie der hohlraumstrahlung). *Mathematische Annalen*, 71(4):441–479, 1912.
- R. F. Woolson. Wilcoxon signed-rank test. *Wiley encyclopedia of clinical trials*, pages 1–3, 2007.
- F. Wu, A. Souza, T. Zhang, C. Fifty, T. Yu, and K. Weinberger. Simplifying graph convolutional networks. In *Proc. Int. Conf. Machine Learning*, 2019.
- D. Xu, W. Cheng, D. Luo, H. Chen, and X. Zhang. InfoGCL: Information-aware graph contrastive learning. In *Proc. Advances in Neural Information Processing Systems*, 2021.
- K. Xu, W. Hu, J. Leskovec, and S. Jegelka. How powerful are graph neural networks? In *Proc. Int. Conf. Learning Representations*, 2019.
- P. Yanardag and S. Vishwanathan. Deep graph kernels. In *Proc. ACM SIGKDD Int. Conf. Knowledge Discovery & Data Mining*, 2015.
- G. Yehudai, E. Fetaya, E. Meir, G. Chechik, and H. Maron. From local structures to size generalization in graph neural networks. In *Proc. Int. Conf. Machine Learning*, pages 11975–11986. PMLR, 2021.
- Z. Ying, J. You, C. Morris, X. Ren, W. Hamilton, and J. Leskovec. Hierarchical graph representation learning with differentiable pooling. In *Proc. Advances in Neural Information Processing Systems*, 2018.
- Y. You, T. Chen, Y. Sui, T. Chen, Z. Wang, and Y. Shen. Graph contrastive learning with augmentations. In *Proc. Advances in Neural Information Processing Systems*, 2020.
- Y. You, T. Chen, Y. Shen, and Z. Wang. Graph contrastive learning automated. In *Proc. Int. Conf. Machine Learning*, pages 12121–12132. PMLR, 2021.
- Y. You, T. Chen, Z. Wang, and Y. Shen. Bringing your own view: Graph contrastive learning without prefabricated data augmentations. In *WSDM*, 2022.
- F. Zhang, X. Liu, J. Tang, Y. Dong, P. Yao, J. Zhang, X. Gu, Y. Wang, B. Shao, R. Li, et al. OAG: Toward linking large-scale heterogeneous entity graphs. In *KDD*, pages 2585–2595, 2019a.
- J. Zhang, J. Tang, C. Ma, H. Tong, Y. Jing, and J. Li. Panther: Fast top-k similarity search on large networks. In *Proc. ACM SIGKDD Int. Conf. Knowledge Discovery & Data Mining*, 2015.
- J. Zhang, X. Shi, J. Xie, H. Ma, I. King, and D.-Y. Yeung. Gaan: Gated attention networks for learning on large and spatiotemporal graphs. *arXiv preprint arXiv:1803.07294*, 2018.
- J. Zhang, Y. Dong, Y. Wang, and J. Tang. Prone: fast and scalable network representation learning. In *Proc. Int. Joint Conf. Artificial Intelligence*, pages 4278–4284, 2019b.
- S. Zhang, Z. Hu, A. Subramonian, and Y. Sun. Motif-driven contrastive learning of graph representations. *arXiv preprint arXiv:2012.12533*, 2020.
- Y. Zhu, Y. Xu, F. Yu, Q. Liu, S. Wu, and L. Wang. Deep graph contrastive representation learning. *arXiv preprint arXiv:2006.04131*, 2020.
- Y. Zhu, Y. Xu, F. Yu, Q. Liu, S. Wu, and L. Wang. Graph contrastive learning with adaptive augmentation. In *WWW*, 2021.

Supplementary Materials for SGCL

List of all contents

- Sections 1 to 3 position our work better and provide references.
- Section 4 has implementation details, ablations, statistical tests, and all other results not in the main text. Section 5 adds confidence intervals and some more results and confidence intervals.
- Section 6 has some results for MNIST and CIFAR-10 to illustrate linkages between our method and image cropping.
- Section 7 discusses limitations, societal impact and reproducibility.
- Section 8 has additional ablations based on spectral properties.
- Section 9 has proofs of some mathematical results used in the paper for various augmentations.
- Section 10 has proofs on the stochastic block model.
- Sections 11, 12, 13 add small details that help explain how the entire suite works. Section 11 has time complexity graphs, section 12 has a case of negative transfer which pops up in some experiments and looks anomalous otherwise, and section 13 visualizes why we need to align two graphs in the first place.

7 Position of our work

We emphasize that there are three distinct cases of consideration in the field of contrastive learning in graphs. We hope to make a clear separation between them to help readers understand our model design and the choice of baselines as well as the datasets we conduct experiments on. A summarizing of the position of our work vs. prior works is presented in Table 5.

Table 5: Detailed analysis of our work vs. existing work

	Pre-train with Freeze encoder (Out of domain)	Pre-train with encoder fine-tune (Out of domain)	Pre-train with Freeze encoder (Same domain)	Pre-train with encoder fine-tune (Same domain)	Unsupervised learning
Training Data	$\{\mathbf{X}_{LP}, \mathbf{A}\}_{\text{pretrain}}$	$\{\mathbf{X}_{LP}, \mathbf{A}\}_{\text{pretrain}}$ $\{\mathbf{X}_{LP}, \mathbf{A}, \mathbf{Y}\}_{\text{downstream}}$	$\{\mathbf{X}, \mathbf{A}\}_{\text{pretrain}}$	$\{\mathbf{X}, \mathbf{A}\}_{\text{pretrain}}$ $\{\mathbf{X}, \mathbf{A}, \mathbf{Y}\}_{\text{downstream}}$	$\{\mathbf{X}, \mathbf{A}\}_{\text{downstream}}$
Methods in the category	Ours, GCC	Ours, GCC	GPT-GNN, GraphCL, MICRO-Graph JOAO, BYOV, GraphMAE	GPT-GNN, GraphCL, MICRO-Graph JOAO, BYOV, GraphMAE	InfoGCL, MVGRL GraphCL, GCA

First, we have out of domain pre-training, where the encoder only sees a large pre-training corpus in the training phase that may share no node attributes at all with the downstream task. A representative method is GCC (Qiu et al., 2020). For example, this pre-training dataset can be a large citation network or social network (as the pre-train corpus used in our paper), while the downstream task may be on a completely different domain such as molecules. Since no node attributes are shared between the two domains, the initial node attributes have to rely solely on structure, e.g., the adjacency or Laplacian matrices and embeddings derived from their eigendecomposition. Importantly, in this case, the encoder is never trained on any labeled or unlabeled instances for the downstream graph related tasks before doing the inference. It allows the model to obtain the results on the downstream task very fast (since only the model inference step is applied to obtain the node representations for the downstream tasks). We call this setting pre-training with frozen encoder (out of domain). This is the most difficult graph contrastive learning (GCL) related task. In our paper, we strictly follow this setup. The downstream task performance can be further improved if the downstream training instances (data, but also possibly with labels) are shown to the GNN encoder. We call this setting pre-training with fine-tuning (out of domain).

Second, we have the domain specific pre-training method where the encoder sees a large pre-training corpus which shares similar features or the same feature tokenization method as the downstream task. The representative methods that fall under this category include GPT-GNN Hu et al. (2020c), GraphCL (You et al., 2020), MICRO-Graph (Zhang et al., 2020), JOAO (You et al., 2021), BYOV (You et al., 2022), and GraphMAE (Hou et al., 2022). The typical experiment design for this setting is to pre-train the GNN encoder on a large-scale bioinformatics dataset, and then fine-tune and evaluate on smaller datasets of the same category. Since the feature space is properly aligned between the pre-train dataset and the downstream datasets, the node attributes usually are fully exploited during the pre-training stage. Similarly, the downstream task performance can be further improved if the downstream tasks (data and/or their labels) are shown to the GNN encoder. We call these two setting pre-training with frozen encoder (same domain) and pre-training with encoder fine-tuning (same domain).

Third, in the unsupervised learning setting for GCL, there is no large pre-training corpus that is distinct from the downstream task data. Rather, the large training set of the downstream task is the sole material for contrastive pre-training. Note that in this case, if there are multiple unrelated downstream tasks, e.g., a citation network and also a molecule task, a separate pre-training procedure must be conducted for each task and a separate network must be trained. The representative methods that fall under this category include InfoGCL (Xu et al., 2021), MVGRL (Hassani and Khasahmadi, 2020), GraphCL (You et al., 2020), GCA (Zhu et al., 2021). Generally speaking, for tasks that rely heavily on the node attributes (such as citations, and molecule graphs), such unsupervised methods, when the training set data (adjacency matrix and node attributes) is available for the unsupervised training phase, can potentially outperform the out of domain pre-trained frozen encoder case. But this is natural, and expected, because in the out-of-domain pre-training with a frozen encoder setting the pre-trained network never even sees the source domain. It can never take advantage of node attributes because the pre-train datasets do not share the same feature space as the downstream task. It can only rely on the potential transferable structural features. But this is also not its purpose - its purpose is to act like a general large language model (LLM) or a Foundation Model like GPT-3. Such a model is not necessarily an expert in every area and can be outperformed by, for instance, specific question-answer-specialized language models for answering questions, but it performs relatively well zero-shot in most tasks without needing any pre-training. This is why in our main paper, we did not compare with the commonly used small-scale datasets (Cora, Citesser) for the unsupervised learning tasks.

Previous papers in this field such as GraphMAE (Hou et al., 2022) often include the frozen, pre-trained models under

the unsupervised category in the experiments, which is not completely accurate or fair. In fact, this category is relatively understudied and introduces unique challenges for the out-of-domain transfer setting. Its importance, and relative lack of study, is precisely why it deserves attention - it is a step toward out-of-domain generalization on graphs and avoids expensive pre-training in every domain. In the following table, we provide a novel way to categorize the existing graph contrastive learning work and we hope it provides better insight to the readers in terms of the position of our work.

Please note that even though not directly applicable for the pre-train (out of domain) mode, for the existing methods under the category of pre-train (same domain) and unsupervised learning, we are able to make modifications to allow them to be applied in the out of domain settings. The main changes are 1) we use the pre-train out of domain corpus $\{\mathbf{X}_{LP}, \mathbf{A}\}_{\text{pretrain}}$ to train the GNN encoder instead of $\{\mathbf{X}, \mathbf{A}\}_{\text{downstream}}$; 2) since the feature space between the pre-train domains and the target domain are not aligned, we use \mathbf{X}_{LP} instead of the original feature \mathbf{X} . We conduct the above modification to some of the existing unsupervised learning based methods such as MVGRL (Hassani and Khasahmadi, 2020) and GraphCL (You et al., 2020). This is also why we cannot, without running the out of domain pre-training experiment setups, directly report the experimental performance in the previous papers (largely unsupervised, except GCC), and why some of our numbers do not always agree with those reported in the original paper, e.g., MVGRL on IMDB-BINARY. The entire training process is completely different with a new pre-training corpus, and the same numbers are not guaranteed to occur.

8 Reasons to pursue augmentations based on graph spectra

First, we want to address the question of what is meant by the term "universal topological properties". Our method is inherently focused on transferring the pre-trained GNN encoder to any domain of graphs, including those that share no node attributes with the pre-train data corpus. This means that the only properties the encoder can use when building its representation are transferable structural clues. We use the word topological to denote this structure-only learning. The word universal denotes the idea of being able to easily transfer from pre-train graphs to any downstream graphs. It is a common practice to augment node descriptors with structural features (Errica et al., 2020), especially for graph classification tasks. DiffPool (Ying et al., 2018) adds the degree and clustering coefficient to each node feature vector. GIN (Xu et al., 2019) adds a one-hot representation of node degrees. In short, a universal topological property is some property such as the human-defined property of "degree" that we hope the GNN will learn in an unsupervised fashion. Just as degree - a very useful attribute to know for any graph for many downstream tasks - is derivable from the adjacency matrix by taking a row sum, we hope the GNN will learn a sequence of operations that distill some concept that is even more meaningful than the degree and other basic graph statistics.

Since structural clues are the only ones that can be transferable between pre-train graphs and the downstream graphs, the next part to answer is why spectral methods, and why should we use the spectral-inspired augmentations to achieve the out-of-domain generalization goal. We elaborate as follows.

For multiple decades, researchers have demonstrated the success of graph spectral signals with respect to preserving the unique structural characteristics of graphs (see (Torres et al., 2020) and references therein). Graph spectral analysis has also been the subject of extensive theoretical study and it has been established that the graph spectral information is important to characterize the graph properties. For example, graph spectral values (such as the Fiedler eigenvalue) related directly to fundamental properties such as graph partitioning properties (Kwok et al., 2013; Lee et al., 2014) and graph connectivity (Chung, 1997; Kahale, 1995; Fiedler, 1973). Spectral analyses of the Laplacian matrix have well-established applications in graph theory, network science, graph mining, and dimensionality reduction for graphs (Torres et al., 2020). They have also been used for important tasks such as clustering (Belkin and Niyogi, 2001; Von Luxburg, 2007b) and sparsification (Spielman and Srivastava, 2008). Moreover, many network embedding methods such as LINE (Tang et al., 2015) and DeepWalk reduce to factorizing a matrix derived from the Laplacian, as addressed in NetMF (Qiu et al., 2018). These graph spectral clues allow us to extract transferable structural features and structural commonality across graphs from different domains. All of these considerations motivate us to use spectral-inspired augmentations for graph contrastive learning to fully exploit the potential universal topological properties across graphs from different domains.

9 Related Work Extension

9.1 Representation learning on graphs

A significant body of research focuses on using graph neural networks to encode both the underlying graph describing relationships between nodes as well as the attributes for each node (Kipf and Welling, 2017; Gilmer et al., 2017; Hamilton

et al., 2017; Veličković et al., 2018; Xu et al., 2019). The core idea for GNNs is to perform feature mapping and recursive neighborhood aggregation based on the local neighborhood using shared aggregation functions. The neighborhood feature mapping and aggregation steps can be parameterized by learnable weights, which together constitute the graph encoder.

There has been a rich vein of literature that discusses how to design an effective graph encoding function that can leverage both node attributes and structure information to learn representations (Kipf and Welling, 2017; Hamilton et al., 2017; Veličković et al., 2018; Zhang et al., 2018; Wu et al., 2019; Chen et al., 2020a; Xu et al., 2019). In particular, we highlight the Graph Isomorphism Network (GIN) (Xu et al., 2019), which is an architecture that is provably one of the most expressive among the class of GNNs and is as powerful as the Weisfeiler Lehman graph isomorphism test. Graph encoding is a crucial component of GNN pre-training and self-supervised learning methods. However, most existing graph encoders are based on message passing and the transformation of the initial node attributes. Such encoders can only capture vertex similarity based on features or node proximity, and are thus restricted to being domain-specific, incapable of achieving transfer to unseen or out-of-distribution graphs. In this work, to circumvent this issue, we employ structural positional encoding to construct the initial node attributes. By focusing on each node’s local subgraph level representation, we can extract universal topological properties that apply across multiple graphs. This endows the resultant graph encoder with the potential to achieve out-of-domain graph data transfer.

9.2 Data augmentations for contrastive learning

Augmentations for image data. Representation learning is of perennial importance in machine learning with contrastive learning being a recent prominent technique. In the field of representation learning for image data, under this framework, there has been an active research theme in terms of defining a set of transformations applied to image samples, which do not change the semantics of the image. Candidate transformations include cropping, resizing, Gaussian blur, rotation, and color distortion. Recent experimental studies (Chen et al., 2020b; Grill et al., 2020) have highlighted that the combination of random crop and color distortion can lead to significantly improved performance for image contrastive learning. Inspired by this observation, we seek analogous graph augmentations.

Augmentations for graph data. The unique nature of graph data means that the augmentation strategy plays a key role in the success of graph contrastive learning (Qiu et al., 2020; You et al., 2020; Li et al., 2021; Sun et al., 2019; Hassani and Khasahmadi, 2020; Xu et al., 2021). Commonly-used graph augmentations include: 1) *attribute dropping or masking* (You et al., 2020; Hu et al., 2020c): these graph feature augmentations rely heavily on domain knowledge and this prevents learning a domain invariant encoder that can transfer to out-of-domain downstream tasks; 2) *random edge/node dropping* (Li et al., 2021; Xu et al., 2021; Zhu et al., 2020, 2021): these augmentations are based on heuristics and they are not tailored to preserve any special graph properties; 3) *graph diffusion* (Hassani and Khasahmadi, 2020): this operation offers a novel way to generate positive samples, but it has a large additional computation cost (Hassani and Khasahmadi, 2020; Page et al., 1999; Kondor and Lafferty, 2002). The graph diffusion operation is more costly than calculation and application of the Personalized Page Rank (PPR) (Page et al., 1999) based transition matrix since it requires an inversion of the adjacency matrix; and 4) *random walks around a center node* (Tong et al., 2006; Qiu et al., 2020): this augmentation creates two independent random walks from each vertex that explore its ego network and these form multiple views (subgraphs) of each node. Additionally, there is an augmentation called GraphCrop (Wang et al., 2020), which uses a node-centric strategy to crop a contiguous subgraph from the original graph while maintaining its connectivity; this is different from the spectral graph cropping we propose. Existing structure augmentation strategies are not tailored to any special graph properties and might unexpectedly change the semantics (Lee et al., 2022).

9.3 Pre-training, self-supervision, unsupervised & contrastive graph representation learning

Though not identical, pre-training, self-supervised learning, and contrastive learning approaches in the graph learning domain use many of the same underlying methods. A simple technique such as attribute masking can, for example, be used in pre-training as a surrogate task of predicting the masked attribute, while in the contrastive learning scenario, the masking is treated as an augmentation. We categorize the existing work into the following 5 categories.

Category 1. One of the early works in the contrastive graph learning direction is Deep Graph Infomax (DGI) (Veličković et al., 2019). Though not formally identified as contrastive learning, the method aims to maximize the mutual information between the patch-level and high-level summaries of a graph, which may be thought of as two views. Infomax is a similar method that uses a GIN (Graph Isomorphism Network) and avoids the costly negative sampling by using batch-wise generation (Sun et al., 2019). MVGRL (Hassani and Khasahmadi, 2020) tackles the case of multiple views, i.e., positive

Table 6: Properties of different approaches to graph contrastive (unsupervised) learning. * indicates that the method was not originally designed for pre-training, but can be trivially adapted to it. **A fuller description with relevant references is added in the appendix.**

Approaches	Goal is pre-training or transfer	No requirement for features	Domain transfer	Shareable graph encoder
Category 1 (DGI, InfoGraph, MVGRL, DGCL, InfoGCL, AFGRL)	✗	✗	✗	✗
Category 2 (GPT-GNN, Strategies for pre-training GNNs)	✓	✗	✗	✓
Category 3 (Deepwalk, LINE, node2vec)	✗	✓	✓	✗
Category 4 (struc2vec, graph2vec, DGK, Graphwave, InfiniteWalk)	✗	✓	✓	✗
Category 5 (GraphCL, CuCo*, GCC, BYOV, GRACE*, GCA*, Ours)	✓	✓	✓	✓

pairs per instance, similar to Contrastive Multiview coding for images. DGCL (Li et al., 2021) adopts a disentanglement approach, ensuring that the representation can be factored into components that capture distinct aspects of the graph. InfoGCL (Xu et al., 2021) learns representations using the Information Bottleneck (IB) to ensure that the views minimize overlapping information while preserving as much label-relevant information as possible. None of the methods in this category is capable of capturing universal topological properties that extend across multiple graphs from different domains.

Category 2. Predicting masked edges/attributes in chemical and biological contexts has emerged as a successful pre-train task. GPT-GNN (Hu et al., 2020c) performs generative pre-training successively over the graph structure and relevant attributes. In (Hu et al., 2020b), Hu et al. propose several strategies (attribute masking, context structure prediction) to pre-train GNNs with joint node-level and graph-level contrastive objectives. This allows the model to better encode domain-specific knowledge. However, the predictive task for these methods relies heavily on the features and domain knowledge. As a result, the methods are not easily applied to general graph learning problems.

Category 3 Random-walk-based embedding methods like Deepwalk (Perozzi et al., 2014), LINE (Tang et al., 2015), and Node2vec (Grover and Leskovec, 2016) are widely used to learn network embeddings in an unsupervised way. The main purpose is to encode the similarity by measuring the proximity between nodes. The embeddings are derived from the skip-gram encoding method, Word2vec, in Natural Language Processing (NLP). However, the proximity similarity information can only be applied within the same graph. Transfer to unseen graphs is challenging since the embeddings learned on different graphs are not naturally aligned.

Category 4 To aid transferring learned representations, another approach of unsupervised learning attempts encoding structural similarities. Two nodes can be structurally similar while belonging to two different graphs. Handcrafted domain knowledge based representative structural patterns are proposed in (Yanardag and Vishwanathan, 2015; Ribeiro et al., 2017; Narayanan et al., 2017). Spectral graph theory provides the foundation for modelling structural similarity in (Qiu et al., 2018; Donnat et al., 2018; Chanpuriya and Musco, 2020).

Category 5 In the domain of explicitly contrastive graph learning, we consider Graph Contrastive Coding (GCC) (Qiu et al., 2020) as the closest approach to our work. In GCC, the core augmentation used is random walk with return (Tong et al., 2006). This forms multiple views (subgraphs) of each node. GraphCL (You et al., 2020) expands this augmentation suite to add node dropping, edge perturbations, and attribute masking. Additionally, although they are not designed for pre-training, we integrated the augmentation strategies from MVGRL (Hassani and Khasahmadi, 2020), Grace (Zhu et al., 2020), Cuco (Chu et al., 2021), and Bringing Your Own View (BYOV) (You et al., 2022) to work with the pre-train setup in category 5.

10 Implementation details, additional results, and ablations

10.1 Codebase references

In general, we follow the code base of GCC (Qiu et al., 2020), provided at : <https://github.com/THUDM/GCC>. We use it as a base for our own implementation (provided along with supplement). Please refer to it in general with this section. For results using struc2vec (Ribeiro et al., 2017), ProNE (Zhang et al., 2019b), Panther (Zhang et al., 2015), RoIX (Henderson et al., 2012) and graphwave (Donnat et al., 2018) we report the results directly from (Qiu et al., 2020) wherever applicable.

10.2 Dataset details

We provide the important details of the pre-training datasets in the main paper, so here we describe the downstream datasets. We obtain US-airport from the core repository of GCC (Qiu et al., 2020) which itself obtains it from (Ribeiro et al., 2017). H-index is obtained from GCC as well via OAG (Zhang et al., 2019a). COLLAB, REDDIT-BINARY, REDDIT-MULTI5K, IMDB-BINARY, IMDB-MULTI all originally derive from the graph kernel benchmarks (Morris et al., 2020), provided at : <https://chrsmrrs.github.io/datasets/>. Finally, the top-k similarity datasets namely KDD-ICDM, SIGIR-CIKM, and SIGMOD-ICDE, are obtained from the GCC repository (Qiu et al., 2020); these were obtained from the original source, Panther (Zhang et al., 2015).

10.3 Hyperparameters and statistical experimental methodology

Hyperparameters: Training occurs over 75,000 steps with a linear ramping-on (over the first 10%) and linear decay (over the last 10%) using the ADAM optimizer, with an initial learning rate of 0.005, $\beta_1 = 0.9$, $\beta_2 = 0.999$, $\epsilon = 10^{-8}$. The random walk return probability is 0.8. The *E2E* dictionary size $K = 1023$, for MoCo 16384. The batch size is 1024 for *E2E* and 32 for MoCo. The dropout is set to 0.5 with a degree embedding of dimension 16 and positional embedding of dimension 64. These hyperparameters are retained from GCC and do not require grid search. The hyperparameter c for alignment is chosen by grid search from 6 values, namely 0.2, 0.25, 0.3, 0.35, 0.4, 0.45.

Runtime: Using DBLP as the test bed, we observed 33.27 seconds per epoch for baseline GCC, which was only increased to at most 41.08 seconds in the settings with the most augmentations. Note that epoch time is largely CPU controlled in our experience and may vary from server to server. However, we found that the ratios between different methods were far more stable. The main paper reports these values on a per graph basis.

Confidence intervals and statistical methodology : To construct confidence bounds around our results, we carry out the following procedure. We introduce some randomness through seeds. The seed is employed twice: once during training the encoder, and again while fine-tuning the encoder on downstream tasks on the datasets. We carry out training with 8 random seeds, resulting in 8 encoders. From each of these encoders, the representation of the graphs in the downstream datasets is extracted.

Next, we train a SVC (for graph datasets) or a logistic regression module (for node datasets), both with a regularization co-efficient over 10 stratified K-fold splits. Before testing the model obtained from the train fraction of any split, we sample uniformly with replacement from the test set of the split of size T until we draw T samples. These instances are graphs (ego-graphs for the case of node datasets and distinct graphs for the case of graph datasets). After this we report the testing result. This is a bootstrapping procedure that leads to a random re-weighting of test samples. This entire process - i.e., generating a new 10-fold split, training, bootstrapping, testing - is repeated 10 times per encoder.

This leads to a total of 800 data points per encoder, allowing fine-grained confidence intervals. However, we found that performance varied too strongly as a function of the splits, leading us to average over the splits instead. Therefore, each determination carries an effective sample size of 80. Upon this, the Whitney-Mann, Wilcoxon signed rank, and t-tests are carried out to determine p-values, 5 to 95 percentile confidence bounds, and standard deviations.

10.4 Augmentation details and sequences

Masking: As mentioned in the main paper, we follow previous work (Hu et al., 2020b) and add simple masking of \mathbf{X}_i . The masking involves setting some columns to zero. Since we consider smaller eigenvalues of \mathbf{L}_i to be more important, we draw an integer z uniformly in the range $[0, M]$ and mask out z eigenvectors corresponding to the top z eigenvalues of \mathbf{L}_i .

Sequence of augmentations: We have discussed the creation of views of G'_i from graph instances G_i . However, in our case, the goal is to create two positive views G'_i, G''_i per mini-batch for an instance G_i . Let us now clarify the sequence of augmentations we employ. It should be understood that for any G_i , the negative view is any augmented or un-augmented view of $G_j, j \neq i$.

- First, we create G'_i, G''_i using random walk with return on G_i . We use the random walk hyperparameters identified in (Qiu et al., 2020).
- With probability p_{filter} , we then test G'_i, G''_i using similarity or diversity thresholds $1-c$ and repeat the first step if the test fails. If G'_i, G''_i do not pass in t_{max} tries, we proceed to the next step.

- We randomly crop both G'_i, G''_i independently with probabilities over different crops c_1, c_2, \dots (including no crop). In total, we allow five outcomes, i.e. $c_1, c_2, c_3, c_4, c_5 = 1 - \sum_{i=1}^4 c_i$. The last outcome is the case of no cropping. We keep $c_1 = c_2, c_3 = c_4$. These correspond to different types of crops, explained below. We can term $c_1 + c_2 + c_3 + c_4$ as p_{crop} .
- With probability p_{align} , we replace $\mathbf{X}'_i, \mathbf{X}''_i$ with $\mathbf{X}'_i \mathbf{Q}^*, \mathbf{X}''_i \mathbf{Q}^{**}$ or keep $\mathbf{X}'_i, \mathbf{X}''_i$ unchanged with probability $1 - p_{align}$.
- We apply one of the mask and reorder augmentations on both G'_i, G''_i independently to form the final positive pairs. That is, for G'_i , we mask it with p_{mask} , or reorder it with $p_{reorder}$, or keep it unchanged with $1 - p_{mask} - p_{reorder}$. The same process is then done, independently, for G''_i .

For a graph G , the $x_{min}, x_{max}, y_{min}, y_{max}$ values for cropping are chosen as follows. We calculate the values taken by the second eigenvector over G and rank them, and set x_{min} on the basis of the rank. That is, $x_{min} = R_{0.2}$ would correspond to x_{min} being set as the 20-th percentile value over G . This is done instead of absolute thresholds to sidestep the changes of the second eigenvector over the different G s. The corresponding different types of crop are, written as R values $[x_{min}, x_{max}, y_{min}, y_{max}]$ tuples :

- $[R_{0.2}, R_{0.8}, R_{0.2}, R_{0.8}]$ with $c_1 = 0.1$
- $[R_{0.1}, R_{0.9}, R_{0.1}, R_{0.9}]$ with $c_2 = 0.1$
- $[R_0, R_{0.8}, R_0, R_{0.8}]$ with $c_3 = 0.05$
- $[R_{0.2}, R_{1.0}, R_{0.2}, R_{1.0}]$ with $c_4 = 0.05$
- No crop, with $c_5 = 0.7$

Note that in terms of alignment augmentations, our arguments regarding $\mathbf{X}'_i, \mathbf{X}''_i$ being transformed to $\mathbf{X}'_i \mathbf{Q}^*, \mathbf{X}''_i \mathbf{Q}^{**}$ as it respects the inner product carry over if we instead use $\mathbf{X}'_i, \mathbf{X}''_i \mathbf{Q}^{**} (\mathbf{Q}^*)^T$ or $\mathbf{X}'_i \mathbf{Q}^* (\mathbf{Q}^{**})^T, \mathbf{X}''_i$ as the augmented views.

Order of augmentations. We have chosen the augmentations to proceed in this order due to the following reasons.

- Of all the candidates for the first augmentation in our sequence, the random walk is supreme as it cuts down on the size of the ego-net for the future steps and the Laplacian eigendecomposition’s complexity as well. Doing away with it greatly increases the runtime for any other step preceding it.
- Filtering is best done as early as possible to reject candidates on its basis before expensive augmentation steps have already been performed. Hence, we place it second.
- Cropping precedes align, mask and ordering as these change the attribute vectors, and cropping uses the second eigenvector which is part of the embedding itself.
- Alignment precedes mask and reorder, as alignment on shifted embeddings post-mask or post-reorder no longer follows from our arguments of its necessity.
- Mask and reorder are mutually exclusive as reordering a masked matrix does not obey the diffusion matrix argument we make for reordering as an augmentation. While masking a diffused matrix is logically allowed, we did not experiment on this case thoroughly and did not find any encouraging preliminary empirical results for this case.

We do not claim our order is the best of all possible permutations. Nevertheless, it can be seen the choice is not entirely ad hoc.

10.5 Ablation tables

The necessity of our spectral crop and reorder frequency components. We first report in Table 1 the results of ablations that involve replacing the proposed crop and reorder augmentations with random analogues. The results validate the necessity of following our eigenspectrum-designed approaches for cropping and reordering. We explore replacing the proposed crop with a random crop (randomly selecting a subgraph by excluding nodes). For reordering, we compare to a random permutation of spectral positional encoding. We observe a consistent drop in performance across all datasets when

Table 1: Ablation study for random versions of crop and permute vs. our spectral cropping and spectral positional encoding permute, E2E only. Bolding means best, asterisk for significance. Statistical analysis and standard deviations in Appendix C.

Augment	US-Airport	H-index	IMDB-B	IMDB-M	COLLAB	RDT-B	RDT-M
GCC	64.8	78.3	71.7	49.3	74.7	87.5	52.6
SGCL - Random Permute	63.5	76.1	71.4	47.8	74.2	86.8	52.2
SGCL - Random Crop	64.5	78.5	71.8	49.4	74.4	87.8	52.1
SGCL	65.3*	78.9	73.0*	49.8	75.6*	88.4*	53.8*

Table 2: Pairwise effect of augmentations and post-processing methods, with E2E, frozen setting, on Reddit-binary, showing raw percentage gains over GCC (Qiu et al., 2020). Further ablations appear in Appendix B. Marked are statistically significant **positives** and **negatives**.

Dataset	S-Crop	Mask	S-Reorder	Align	Similar	Diverse
S-Crop	0.22	0.47	0.43	0.54	0.71	-0.38
Mask		0.15	0.26	0.35	0.42	-0.15
S-Reorder			0.18	0.19	0.58	0.45
Align				0.16	0.56	-0.26
Similar					0.31	N/A
Diverse						-0.72

we replace either augmentation with its random counterpart. This indicates that our spectral augmentation designs can make a significant difference in terms of capturing more effective universal topological properties.

In this section we now report the results for all other datasets when subjected to pairwise augmentations. We do want to re-iterate that since we have ten downstream datasets and five large-scale pre-train datasets, we select Reddit-binary as the downstream task and the smallest pre-train DBLP (SNAP) dataset as a demonstration. Using more pre-train datasets should result in further performance improvements, but due to computation time constraints, we focus on the simpler setting. We present these results (raw percentage gains over GCC) in tables 2,3,4,5,6,7,8. Statistically **positive** and **negative** cases are marked accordingly.

Dataset	Crop	Mask	Reorder	Align	Similar	Diverse
Crop	0.62	0.58	0.55	0.43	0.85	0.32
Mask		-0.24	-0.56	-1.04	0.52	-0.17
Reorder			-0.14	-0.49	0.38	-0.26
Align				-0.47	0.64	-0.56
Similar					0.45	N/A
Diverse						-0.59

Table 3: Ablation results on Reddit-5K

Spectral Augmentations for Graph Contrastive Learning

Dataset	Crop	Mask	Reorder	Align	Similar	Diverse
Crop	0.83	0.92	1.16	0.98	0.87	0.62
Mask		-0.32	0.58	0.22	-0.35	-0.78
Reorder			0.75	0.82	0.56	0.43
Align				0.18	-0.19	-0.22
Similar					-0.08	N/A
Diverse						-0.15

Table 4: Ablation results on IMDB-Binary

Dataset	Crop	Mask	Reorder	Align	Similar	Diverse
Crop	0.24	0.42	0.56	0.47	0.38	0.31
Mask		0.31	0.52	0.43	0.25	0.38
Reorder			0.48	0.38	0.21	0.34
Align				0.28	0.20	0.36
Similar					-0.11	N/A
Diverse						0.06

Table 5: Ablation results on h-index dataset

Dataset	Crop	Mask	Reorder	Align	Similar	Diverse
Crop	-0.08	0.27	-0.18	-0.43	0.28	0.22
Mask		0.31	0.26	0.16	0.43	0.38
Reorder			-0.15	-0.23	-0.07	0.03
Align				-0.12	0.14	0.05
Similar					0.25	N/A
Diverse						0.14

Table 6: Ablation results on US-Airport dataset

Dataset	Crop	Mask	Reorder	Align	Similar	Diverse
Crop	0.23	0.42	0.32	0.34	0.71	0.54
Mask		0.18	0.45	0.32	0.62	0.42
Reorder			0.22	0.45	0.55	0.59
Align				0.15	0.68	0.52
Similar					0.48	N/A
Diverse						0.34

Table 7: Ablation results on COLLAB dataset

Dataset	Crop	Mask	Reorder	Align	Similar	Diverse
Crop	0.35	0.25	0.48	0.21	0.57	0.66
Mask		-0.07	0.22	-0.19	0.22	0.47
Reorder			0.28	0.17	0.38	0.82
Align				-0.11	0.16	0.54
Similar					0.19	N/A
Diverse						0.62

Table 8: Ablation results on IMDB-Multi dataset

10.6 Additional results with MoCo and Fine-tuning

Pre-trained encoders fine-tuned using ADAM with 3 epochs warmup and 3 epochs ramp-down with a learning rate of 0.005 are used for the fine-tuned case. These results appear in tables 9, 10 and 11. We present results for E2E and MoCo (He et al., 2020) in both the frozen and fine-tuned setting.

Table 9: Node classification. Results obtained by pretraining along with fine-tuning on the downstream dataset labels for both E2E and MoCo, with frozen results also re-provided from the main paper. Statistical details are discussed in Appendix C. The methods that appear above the “Frozen” category are compared relative to frozen methods. They require no fine-tuning and are more similar to frozen methods, however they are distinct in that they are not pre-training heavy but rather extract the structure directly like Laplacian methods, making them distinct but strong baselines with the least requirement in terms of pre-training or data-specific work. Thus, there forms a continuum from these methods to fully fine-tuned methods with frozen methods lying in an intermediate position.

	US-Airport		H-index	
$ V $	1,190		5,000	
$ E $	13,599		44,020	
Frozen-like methods				
ProNE	62.3		69.1	
GraphWave	60.2		70.3	
Struc2vec	66.2		≥ 1 Day	
Frozen				
Training mode	MoCo	E2E	MoCo	E2E
GCC	65.6	64.8	75.2	78.3
GraphCL	62.8	63.5	74.3	76.5
GRACE	62.6	63.3	74.5	77.0
MVGRL	65.2	64.5	75.1	78.1
CuCo	64.9	64.3	75.3	78.2
BYOV	65.3	64.7	76.0	78.1
InfoGCL	63.2	64.1	75.4	77.6
GCA	64.5	64.3	75.8	78.0
SGCL	65.9	65.3	76.7	78.9*
Fine-tuned				
Training mode	MoCo	E2E	MoCo	E2E
GCC	67.2	68.3	80.6	80.5
GraphCL	64.3	66.4	79.0	78.8
GRACE	64.0	65.9	78.2	78.5
MVGRL	66.5	67.9	79.6	79.9
CuCo	66.1	67.7	79.4	80.1
BYOV	67.0	67.8	80.3	80.2
InfoGCL	65.5	67.2	79.8	79.5
GCA	66.8	67.6	80.0	79.9
SGCL	67.5	68.6	80.8	80.7

Table 10: Graph classification results when the pre-trained graph encoder transfers to an out-of-domain graph or is fine tuned. "-" indicates the model is unable to produce reasonable results given 24 hours of training time, as explained in (Qiu et al., 2020). Bolding indicates best result, asterisk indicates statistical significance. Standard deviations, confidence intervals etc. in Appendix C. The methods that appear above the "Frozen" category are compared relative to frozen methods. They require no fine-tuning and are more similar to frozen methods, however they are distinct in that they are not pre-training heavy but rather extract the structure directly like Laplacian methods, making them distinct but strong baselines with the least requirement in terms of pre-training or data-specific work. Thus, there forms a continuum from these methods to fully fine-tuned methods with frozen methods lying in an intermediate position.

Datasets	IMDB-B	IMDB-M	COLLAB	RDT-B	RDT-M					
# graphs	1,000	1,500	5,000	2,000	5,000					
# classes	2	3	3	2	5					
Avg. # nodes	19.8	13.0	74.5	429.6	508.5					
Frozen-like methods										
DGK	67.0	44.6	73.1	78.0	41.3					
graph2vec	71.1	50.4	-	75.8	47.9					
InfoGraph	73.0	49.7	-	82.5	53.5					
Frozen										
Training mode	MoCo	E2E	MoCo	E2E	MoCo	E2E	MoCo	E2E	MoCo	E2E
GCC	72.0	71.7	49.4	49.3	78.9	74.7	89.8	87.5	53.7	52.6
GraphCL	72.2	70.9	49.3	47.9	77.2	74.1	88.7	87.2	52.9	51.8
GRACE	71.7	71.5	49.2	48.8	78.3	74.5	89.2	87.0	53.4	52.0
CuCo	71.8	71.3	48.7	48.5	78.5	74.2	89.3	87.8	52.5	51.6
BYOV	72.3	72.0	48.5	49.2	78.4	75.1	89.5	87.9	53.6	53.0
MVGRL	72.3	72.2	49.2	49.4	78.6	75.0	89.6	87.4	53.4	52.8
InfoGCL	72.0	71.0	48.8	48.2	77.8	74.6	89.1	87.3	52.7	52.2
GCA	72.2	71.9	49.0	48.7	78.4	74.4	88.9	87.5	53.2	52.4
SGCL	73.4*	73.0	50.0	49.8	79.7*	75.6	90.6*	88.4	54.2*	53.8
Fine-tuned										
Training mode	MoCo	E2E	MoCo	E2E	MoCo	E2E	MoCo	E2E	MoCo	E2E
DGCNN		70.0		47.8		73.7		-		-
GIN		75.6*		51.5*		80.2		89.4*		54.5
GCC(Random)		75.6		50.9		79.4		87.8		52.1
GCC	73.8	70.8	50.3	48.5	81.1	79.0	87.6	86.4	53.0	47.4
GraphCL	73.5	71.1	49.8	47.9	80.6	78.6	87.1	86.7	51.9	48.7
GRACE	73.0	71.3	49.4	47.4	79.5	77.6	86.5	86.7	51.5	48.3
CuCo	72.6	71.2	49.2	46.9	78.1	77.0	86.8	86.5	51.3	48.3
BYOV	73.5	72.4	50.1	49.6	81.2	79.3	88.2	87.0	53.9	50.2
MVGRL	72.3	72.2	49.2	49.4	78.6	77.3	87.9	86.8	53.4	49.8
InfoGCL	73.6	71.5	50.0	48.4	80.2	78.8	87.5	86.3	52.4	49.2
GCA	73.1	71.7	49.5	47.9	79.8	78.2	88.0	86.5	52.1	48.6
SGCL	74.2	72.8	50.6	50.1	81.5*	79.8	88.5	87.4	54.4	50.8

Table 11: Top- k similarity search ($k = 20, 40$), frozen cases only with 4 structural methods (Random, RolX, Panther, GraphWave) that are also similar to frozen methods in runtime requirements (see previous tables). Bolding indicates best result, asterisk indicates statistical significance. Standard deviations, confidence intervals etc. in Appendix C.

	KDD-ICDM		SIGIR-CIKM		SIGMOD-ICDE	
$ V $	2,867	2,607	2,851	3,548	2,616	2,559
$ E $	7,637	4,774	6,354	7,076	8,304	6,668
# ground truth		697		874		898
k	20	40	20	40	20	40
Frozen-like methods						
Random	0.0198	0.0566	0.0223	0.0447	0.0221	0.0521
RolX	0.0779	0.1288	0.0548	0.0984	0.0776	0.1309
Panther++	0.0892	0.1558	0.0782	0.1185	0.0921	0.1320
GraphWave	0.0846	0.1693	0.0549	0.0995	0.0947	0.1470
E2E						
GCC	0.1047	0.1564	0.0549	0.1247	0.0835	0.1336
GraphCL	0.0986	0.1574	0.0583	0.1209	0.0796	0.1205
GRACE	0.1021	0.1558	0.0568	0.1226	0.0864	0.1262
MVGRL	0.0982	0.1483	0.0514	0.1174	0.0774	0.1159
CuCo	0.1063	0.1543	0.0568	0.1274	0.0924	0.1374
BYOV	0.1068	0.1585	0.0592	0.1268	0.0824	0.1318
InfoGCL	0.0972	0.1550	0.0595	0.1217	0.0802	0.1237
GCA	0.1007	0.1563	0.0559	0.1197	0.0849	0.1244
SGCL	0.1105*	0.1642	0.0658	0.1363*	0.1076*	0.1561*
MoCo						
GCC	0.0904	0.1521	0.0652	0.1178	0.0846	0.1425
GraphCL	0.0835	0.1507	0.0629	0.1165	0.0872	0.1434
GRACE	0.0852	0.1516	0.0616	0.1172	0.0917	0.1469
MVGRL	0.0826	0.1458	0.0559	0.1116	0.0851	0.1387
CuCo	0.0864	0.1512	0.0624	0.1216	0.0877	0.1414
BYOV	0.0926	0.1553	0.0642	0.1228	0.0859	0.1468
InfoGCL	0.0848	0.1536	0.0619	0.1183	0.0884	0.1425
GCA	0.0843	0.1507	0.0607	0.1192	0.0865	0.1426
SGCL	0.0978*	0.1627	0.0765	0.1306*	0.1049*	0.1583*

10.7 Datasets and benchmark code

We obtain the datasets from the following sources :

- <https://github.com/leoribeiro/struc2vec/tree/master/graph>
- <https://www.openacademic.ai/oag/>
- <https://ls11-www.cs.tu-dortmund.de/staff/morris/graphkerneldatasets>

And the relevant benchmarks from :

- GCC : <https://github.com/THUDM/GCC>
- GraphCL : <https://github.com/Shen-Lab/GraphCL>
- MVGRL : <https://github.com/kavehhassani/mvgrl>
- BYOV : https://github.com/Shen-Lab/GraphCL_Automated
- CuCo : <https://github.com/BUPT-GAMMA/CuCo>
- GRACE : <https://github.com/CRIPAC-DIG/GRACE>

11 Hardware details and statistical confidence intervals of results

Hardware and software: We tested all code on Python 3.7 with PyTorch 1.3.1, CUDA 10.1, scikit-learn 0.20.3. The Tesla V100 (one per model per run) served as the GPU.

We compute statistical confidence bounds only for the methods whose results we do not copy over from the GCC paper.

Table 12: Node classification. Results indicate the upper confidence bound (95 percentile) and the lower (5th percentile) and the standard deviation in brackets.

	US-Airport		H-index	
$ V $	1,190		5,000	
$ E $	13,599		44,020	
Training mode	MoCo	E2E	MoCo	E2E
GraphCL	63.7(0.4) 62.2	64.2(0.3) 62.8	73.9(0.4) 75.2	77.8(0.9) 75.4
GRACE	63.5(0.4) 61.9	63.9(0.3) 62.7	74.1(0.3) 74.9	77.9(0.6) 76.0
MVGRL	65.5(0.2) 64.9	64.7(0.1) 64.3	75.5(0.2) 74.8	78.4(0.2) 77.7
CuCo	65.2(0.2) 64.5	64.6(0.2) 63.9	75.9(0.3) 74.8	78.5(0.2) 77.8
BYOV	65.5(0.2) 64.9	65.2(0.4) 64.6	76.6(0.3) 75.5	78.5(0.3) 77.6
InfoGCL	63.6(0.3) 62.7	64.4(0.2) 63.7	75.8(0.3) 74.9	78.0(0.3) 77.1
GCA	64.9(0.3) 64.0	64.6(0.2) 64.0	76.2(0.3) 75.4	78.3(0.2) 77.6
SGCL	66.2(0.2) 65.7	65.6(0.2) 65.1	77.1(0.3) 76.3	79.1(0.2) 78.7
Fine-tuned				
Training mode	MoCo	E2E	MoCo	E2E
GraphCL	66.6(1.1) 62.9	67.5(0.7) 65.6	78.2(0.5) 79.8	79.5(0.5) 77.9
GRACE	65.1(0.8) 62.8	66.2(0.3) 65.5	78.6(0.4) 77.5	78.8(0.2) 78.1
MVGRL	66.8(0.2) 66.1	68.1(0.2) 67.6	79.7(0.1) 79.4	80.2(0.2) 79.5
CuCo	66.5(0.3) 65.6	68.0(0.3) 67.3	79.7(0.2) 79.0	80.2(0.1) 79.8
BYOV	67.4(0.3) 66.5	68.2(0.3) 67.3	80.5(0.2) 80.0	80.4(0.2) 79.9
InfoGCL	65.9(0.3) 65.0	67.6(0.3) 66.7	79.5(0.2) 80.0	79.9(0.3) 79.0
GCA	67.2(0.3) 66.3	67.9(0.2) 67.3	80.2(0.2) 79.7	80.2(0.3) 79.5
SGCL	67.6(0.1) 67.4	68.8(0.1) 68.5	81.0(0.1) 80.7	80.8(0.1) 80.6

Spectral Augmentations for Graph Contrastive Learning

Table 13: Graph classification confidence bounds. Results indicate the upper confidence bound (95 percentile) and the lower (5th percentile) and the standard deviation in brackets.

Datasets	IMDB-B		IMDB-M		COLLAB		RDT-B		RDT-M	
# graphs	1,000		1,500		5,000		2,000		5,000	
# classes	2		3		3		2		5	
Avg. # nodes	19.8		13.0		74.5		429.6		508.5	

Frozen												
Training mode	MoCo		E2E		MoCo		E2E		MoCo		E2E	
GraphCL	72.8(0.5)	72.1(0.9)	50.1(0.2)	48.4(0.4)	77.5(0.3)	74.7(0.4)	89.3(0.5)	87.7(0.5)	53.5(0.5)	52.8(0.7)	52.8(0.7)	50.7(0.5)
GRACE	72.2(0.4)	71.9(0.3)	49.7(0.3)	49.4(0.5)	78.0(0.2)	75.0(0.3)	89.5(0.2)	87.4(0.3)	53.8(0.3)	53.8(0.3)	52.7(0.5)	51.2(0.5)
CuCo	72.3(0.4)	71.9(0.4)	48.3(0.3)	48.0(0.3)	78.9(0.3)	74.6(0.3)	89.6(0.2)	88.1(0.2)	53.1(0.4)	53.1(0.4)	52.1(0.4)	51.0(0.4)
BYOV	72.6(0.2)	72.3(0.3)	49.1(0.4)	49.6(0.4)	79.1(0.5)	75.3(0.2)	89.9(0.2)	88.2(0.2)	53.9(0.2)	53.9(0.2)	53.3(0.2)	52.6(0.2)
MVGRL	72.7(0.2)	72.6(0.3)	49.5(0.2)	49.8(0.3)	78.8(0.2)	75.4(0.3)	89.9(0.2)	87.7(0.2)	53.6(0.2)	53.6(0.2)	53.1(0.2)	52.5(0.2)
InfoGCL	72.4(0.2)	71.3(0.2)	49.1(0.2)	48.5(0.2)	78.1(0.2)	75.1(0.3)	89.5(0.3)	87.6(0.3)	53.0(0.2)	53.0(0.2)	52.6(0.2)	51.9(0.2)
GCA	72.6(0.2)	72.2(0.2)	49.3(0.2)	49.0(0.2)	78.6(0.2)	74.7(0.2)	89.2(0.3)	87.7(0.2)	53.4(0.2)	53.4(0.2)	52.7(0.3)	52.0(0.3)
SGCL	73.8(0.3)	73.2(0.1)	50.2(0.1)	50.0(0.2)	79.9(0.1)	75.9(0.2)	90.8(0.1)	88.7(0.2)	54.4(0.1)	54.4(0.1)	54.1(0.2)	53.5(0.2)

Fine-tuned												
Training mode	MoCo		E2E		MoCo		E2E		MoCo		E2E	
GraphCL	74.1(0.4)	71.6(0.3)	50.4(0.3)	48.8(0.5)	81.1(0.3)	79.3(0.4)	87.7(0.5)	87.3(0.3)	52.7(0.5)	52.7(0.5)	49.5(0.5)	47.8(0.5)
GRACE	73.6(0.4)	71.7(0.2)	49.8(0.2)	47.7(0.2)	79.8(0.2)	77.9(0.2)	86.9(0.3)	87.1(0.4)	51.8(0.3)	51.8(0.3)	48.7(0.3)	47.9(0.3)
CuCo	73.1(0.3)	71.4(0.2)	49.5(0.2)	47.7(0.2)	78.4(0.2)	77.8(0.6)	87.0(0.5)	87.0(0.4)	51.6(0.2)	51.6(0.2)	48.9(0.4)	47.8(0.4)
BYOV	73.8(0.3)	72.1(0.2)	50.4(0.3)	49.9(0.2)	81.4(0.2)	79.7(0.2)	88.6(0.2)	87.4(0.3)	54.2(0.2)	54.2(0.2)	50.5(0.2)	49.8(0.2)
MVGRL	72.9(0.4)	72.6(0.4)	49.6(0.4)	49.9(0.4)	78.9(0.2)	77.8(0.3)	88.2(0.3)	87.2(0.3)	53.7(0.2)	53.7(0.2)	50.2(0.2)	49.3(0.3)
InfoGCL	73.8(0.1)	71.9(0.3)	50.2(0.2)	48.0(0.2)	80.5(0.3)	79.1(0.2)	87.9(0.3)	86.6(0.2)	52.7(0.2)	52.7(0.2)	49.5(0.2)	49.0(0.2)
GCA	73.3(0.2)	72.1(0.3)	49.8(0.2)	48.5(0.4)	80.2(0.3)	78.5(0.2)	88.2(0.2)	86.9(0.3)	52.5(0.3)	52.5(0.3)	49.0(0.3)	48.1(0.3)
SGCL	74.4(0.1)	73.4(0.3)	50.7(0.1)	50.2(0.1)	81.6(0.1)	80.3(0.2)	88.7(0.1)	87.6(0.2)	54.6(0.1)	54.6(0.1)	51.4(0.4)	50.3(0.4)

Table 14: Top- k similarity search ($k = 20, 40$), frozen cases only, 5-95 intervals with standard deviations in brackets.

	KDD-ICDM		SIGIR-CIKM		SIGMOD-ICDE			
$ V $	2,867		2,607		2,559			
$ E $	7,637		4,774		6,668			
# ground truth			697		898			
k	20		40		20		40	
GraphCL	0.1062 (0.0033)	0.1604 (0.0016)	0.0622 (0.0024)	0.1259 (0.0031)	0.0871 (0.0048)	0.1294 (0.0042)	0.1294 (0.0042)	0.1294 (0.0042)
GRACE	0.0912 (0.0037)	0.1587 (0.0022)	0.0552 (0.0035)	0.1317 (0.0041)	0.0955 (0.0057)	0.1287 (0.0012)	0.1287 (0.0012)	0.1287 (0.0012)
MVGRL	0.1032 (0.0028)	0.1554 (0.0041)	0.0582 (0.0038)	0.1285 (0.0058)	0.0875 (0.0062)	0.1194 (0.0025)	0.1194 (0.0025)	0.1194 (0.0025)
CuCo	0.1091 (0.0026)	0.1591 (0.0031)	0.0634 (0.0040)	0.1342 (0.0038)	0.1028 (0.0052)	0.1508 (0.0081)	0.1508 (0.0081)	0.1508 (0.0081)
BYOV	0.1088 (0.0019)	0.1612 (0.0028)	0.0649 (0.0029)	0.1338 (0.0038)	0.0978 (0.0102)	0.1417 (0.0068)	0.1417 (0.0068)	0.1417 (0.0068)
InfoGCL	0.1031 (0.0038)	0.1592 (0.0032)	0.0628 (0.0026)	0.1286 (0.0047)	0.0847 (0.0035)	0.1292 (0.0043)	0.1292 (0.0043)	0.1292 (0.0043)
GCA	0.1056 (0.0034)	0.1592 (0.0027)	0.0587 (0.0025)	0.1254 (0.0035)	0.0916 (0.0048)	0.1383 (0.0092)	0.1383 (0.0092)	0.1383 (0.0092)
SGCL	0.1137 (0.0024)	0.1675 (0.0028)	0.0721 (0.0042)	0.1426 (0.0046)	0.1124 (0.0028)	0.1615 (0.0035)	0.1615 (0.0035)	0.1615 (0.0035)

MoCo							
GraphCL	0.0877 (0.0038)	0.1561 (0.0031)	0.0656 (0.0018)	0.1198 (0.0021)	0.0918 (0.0021)	0.1479 (0.0029)	0.1479 (0.0029)
GRACE	0.0895 (0.0026)	0.1605 (0.0051)	0.0702 (0.0046)	0.1258 (0.0042)	0.0982 (0.0049)	0.1552 (0.0058)	0.1552 (0.0058)
MVGRL	0.0874 (0.0028)	0.1522 (0.0037)	0.0622 (0.0036)	0.1288 (0.0074)	0.0902 (0.0036)	0.1437 (0.0037)	0.1437 (0.0037)
CuCo	0.0895 (0.0019)	0.1582 (0.0052)	0.0691 (0.0045)	0.1295 (0.0052)	0.0988 (0.0061)	0.1532 (0.0072)	0.1532 (0.0072)
BYOV	0.0962 (0.0019)	0.1596 (0.0027)	0.0688 (0.0027)	0.1269 (0.0020)	0.1022 (0.0082)	0.1559 (0.0058)	0.1559 (0.0058)
InfoGCL	0.0895 (0.0047)	0.1582 (0.0038)	0.0652 (0.0023)	0.1224 (0.0027)	0.0922 (0.0028)	0.1463 (0.0037)	0.1463 (0.0037)
GCA	0.0885 (0.0024)	0.1528 (0.0017)	0.0648 (0.0031)	0.1246 (0.0029)	0.0898 (0.0024)	0.1455 (0.0018)	0.1455 (0.0018)
SGCL	0.1058 (0.0045)	0.1703 (0.0041)	0.0816 (0.0037)	0.1347 (0.0029)	0.1093 (0.0028)	0.1628 (0.0031)	0.1628 (0.0031)

12 Auxiliary experiments on OGB datasets, MNIST and CIFAR-10

12.1 MNIST and CIFAR-10 motivation - implicit assumptions for the crop augment

We now revisit the chain of reasoning that motivates the crop augmentation, enumerated below sequentially :

- Images are a very important, naturally occurring subclass of attributed grid graphs (products of line graphs). Indeed, for any grid graph, assigning the nodes a 3-dimensional attribute corresponding to the RGB intensity assigns the colour part of the image. For the spatial aspect, every grid graph is enumerable in the indices of its constituent line graphs that it is a product of, i.e. we may denote a node of the grid graph as $v_{i,j}$ where $1 \leq i \leq m, 1 \leq j \leq n$ for a grid graph that is the product of two line graphs with m, n nodes. Associate $x_{i,j}, y_{i,j}$ with every such $v_{i,j}$, with the condition that :

$$x_{i,j+1} - x_{i,j} = x_{i,j} - x_{i,j-1}$$

$$y_{i+1,j} - y_{i,j} = y_{i,j} - y_{i-1,j}$$

Clearly, then, every image can be expressed as a grid graph, while the converse is not true. We assume that this generalization is meaningful - after all, an image of shape (m, n) can equally be flattened and written as a 1-dimensional sequence with its dimensions appended separately, yielding a length of $mn + 2$ per channel. Every image can be expressed this way while not every 1d sequence of length $mn + 2$ can be formed into an image, making this a generalization. **We need to demonstrate that the grid graph form of generalizing what an image is, turns out to be more meaningful via some metric than, for example, ad hoc flattening.**

- The crop operation in images, when they are considered equivalent to grid graphs, is equivalent to a value-based thresholding on nodes, depending on the values induced on them using the first two eigenvectors corresponding to the first two nonzero eigenvalues of the Laplacian. This is indeed true, ignoring numerical errors in the eigendecomposition, when the dimensions m, n with $m > n$ of the image are such that $2n > m$. However, the crop operation for images happens to be functional even when $2n > m$, which is not true for the eigenvector-based cropping we propose.
- The crop augment is known to be - practically and empirically - a runaway success among the candidate augmentations in contrastive learning so far, when the representations to be learnt are to be evaluated for image classification.
- Clearly, if the image is to be thought of as a graph, the corresponding expectation is that our proposed graph-level crop succeed for graph classification. Therefore, we investigate if value thresholding based on the two eigenvectors, which is strictly a generalization of the crop operation, is a similar success on graphs in general.

What are the questionable steps taken above ? First, using the first two eigenvectors is one of infinitely many generalizations possible of the crop augmentation. We cannot investigate all such generalizations, but we can instead check if this particular generalization continues to hold when the domain (images) is perturbed.

Secondly, to what extent is an image actually a grid graph ? Does such a generalization remove key aspects of the image ?

We can see that for the latter assumption, a start would be to consider the image classification tasks such as the ubiquitous tasks on MNIST and CIFAR-10, and turn them instead into graph classification tasks, after converting the images into grid graphs. If this process makes the task hopeless, the assumption is assuredly more questionable.

In fact, such benchmarking (Dwivedi et al., 2020) on MNIST and CIFAR-10 has already been carried out with Graph neural networks. The accuracy obtained is close to 100% for MNIST, and above 65% for CIFAR-10, which, while not exceptional, clearly shows that some reasonable information is retained relevant to the class labels by converting images to a grid graph.

Importantly, given such a grid graph, the nodes i.e. the pixels are initialized with their positions for such a graph classification task. We recall from our discussion of the spectra of grid graphs, that it is precisely the (x, y) positions that will be recovered via the two relevant eigenvectors.

If our generalization is correct, then we expect that at the point of generalization - i.e. in the original domain, the generalization and the specific operation it is generalizing (crop) will be identical operations. We now need to change the domain as slightly as possible to the level where the generalization remains valid, but the specific operation can no longer be performed.

This is easily achievable by replacing images (grid graphs) with their **subgraphs** and assuming we have no clue how these graphs came to be (an usual assumption made for graph datasets). Recall that the (x, y) positions to grid graphs were assigned using the knowledge that they were images. However, if we do not know that they are images, we can only use their adjacency matrices.

In the case of the complete grid graph, the adjacency matrix will be enough to recover the (x, y) co-ordinates of each pixel. However, for a subgraph, the two eigenvectors induce different values that need not correlate to (x, y) co-ordinates.

Recall that we have claimed that the values induced by these eigenvectors are useful for segmenting (selecting subgraphs from) graphs of arbitrary kinds for contrastive learning in the view creation process, using the images as an example. If they are useful for arbitrary graphs as our graph classification benchmarks indicate, they must be useful for slightly perturbed (transformed into subgraph) version of images. It should be understood that we are talking of usefulness solely in the sense of learning optimal representations for downstream classification tasks. If they cannot even succeed at this, then our reasoning is likely to be questionable.

Therefore, if the first two eigenvectors yield a positional encoding that is useful for the image classification task when the images are transformed into grid graphs and then made subgraphs of, the results will be consistent with our assumptions. Further, since the image has only meaningful co-ordinates upto 2 axes, we expect no benefits for increasing the dimensionality of such spectral embeddings beyond 2.

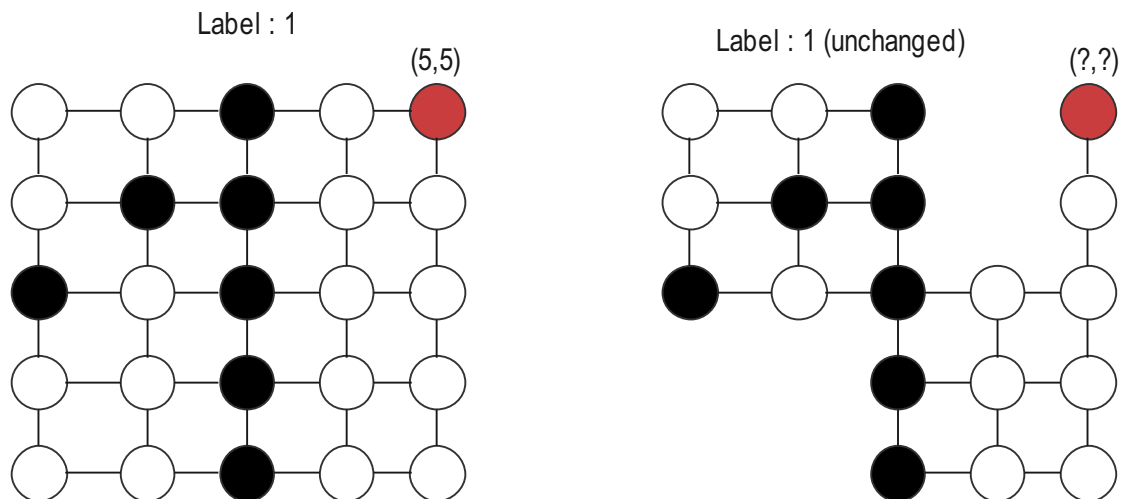


Figure 1: The layout of the subgraph classification experiment, as designed for MNIST. The aim of positional encoding is to give the node (red) a two-dimensional embedding that is as useful to find the label (1) as its initial (x, y) co-ordinate pairing of $(5, 5)$ with 1-indexing. If the first two eigenvectors suffice, they are valid replacements for the axes and yield meaningful embeddings even when the graph is no longer a perfect grid, and this will be reflected in higher accuracy. We assume that for images, a meaningful embedding must at least capture some positional information and thus eigenvector embeddings, if they work, will be validated in generalizing axis-based co-ordinates.

Nature of testing

We consider the following cases, on top of a previously investigated baseline scenario, where each image is converted to a grid graph and each pixel to a node, with edges between adjacent pixels, and the node attribute is 1 or 3 dimensional respectively for MNIST and CIFAR-10, to which 2 dimensions are added via the Laplacian decomposition's eigenvectors corresponding to first two nonzero eigenvalues, bringing the problem into a graph classification problem, where a GCN (5-layer GIN of the same architecture for consistency) is used to process this grid graph, and the node-level representations pooled.

The variants we investigate are :

- Keeping every graph as-is
- Replacing each graph with a subgraph, which consists of the nodes visited by a random walk starting from the center of each graph, taking 512 steps with a return probability of 0.1
- Performing the subgraph step with a random graph crop on top of each subgraph, to simulate our augment scenario.
- Change the positional embedding to either be absent, have only the first dimension, or have 5 dimensions.

In each of the following tables, namely tables 15, 16, 17, 18 for MNIST and 19, 20, 21, 22 for CIFAR-10, rows signify train sets, and columns signify test sets in terms of the modifications performed on them. Overall, we see the same pattern. The random walk, or the subsequent cropping, do not significantly harm the accuracy. There are large gains from going from 0-dimensional positional embeddings to 1, smaller ones from 1 to 2 and beyond 2, a significant drop at 5. **This matches what we expect and justifies our assumptions.**

	Original	Random Walk	Random Walk + Crop
Original	97.8	94.3	89.5
Random Walk	93.2	93.4	88.9
Random Walk + Crop	92.7	91.5	92.8

Table 15: MNIST, 2-dimensional embedding

	Original	Random Walk	Random Walk + Crop
Original	94.2	87.4	85.6
Random Walk	86.5	85.1	83.5
Random Walk + Crop	83.2	81.2	85.9

Table 16: MNIST, 1-dimensional embedding

	Original	Random Walk	Random Walk + Crop
Original	68.9	61.5	58.8
Random Walk	62.4	55.6	53.2
Random Walk + Crop	61.9	54.4	52.6

Table 17: MNIST, 0-dimensional embedding

	Original	Random Walk	Random Walk + Crop
Original	95.6	93.2	87.2
Random Walk	91.5	84.2	84.5
Random Walk + Crop	91.9	86.5	83.8

Table 18: MNIST, 5-dimensional embedding

	Original	Random Walk	Random Walk + Crop
Original	59.5	56.8	55.9
Random Walk	56.2	53.7	53.9
Random Walk + Crop	54.6	52.9	54.3

Table 19: CIFAR-10, 2-dimensional embedding

	Original	Random Walk	Random Walk + Crop
Original	55.4	49.7	52.3
Random Walk	54.2	51.2	50.8
Random Walk + Crop	53.2	47.8	53.2

Table 20: CIFAR-10, 1-dimensional embedding

	Original	Random Walk	Random Walk + Crop
Original	46.9	41.5	43.2
Random Walk	39.8	39.6	40.5
Random Walk + Crop	43.7	38.8	40.2

Table 21: CIFAR-10, 0-dimensional embedding

	Original	Random Walk	Random Walk + Crop
Original	52.7	51.0	53.5
Random Walk	52.4	49.6	51.0
Random Walk + Crop	51.3	50.5	50.2

Table 22: CIFAR-10, 5-dimensional embedding

12.2 Results on OGB datasets of Arxiv (accuracy) and molhiv (HIV) (ROC-AUC)

We also tested our pre-trained models on datasets associated with the Open Graph Benchmark aka OGB (Hu et al., 2020a). Here, the entire test occurs in the fine-tuned setting. We observed some mild benefits associated with pre-training over the common sense GIN benchmark, even when both networks had the advantage of utilizing the structural embedding (Recall, of course, that only the structural embedding aspect can transfer between widely divergent datasets that share no attributes otherwise). These results are summarized in table 23.

	Arxiv	HIV
GIN - Attr + Struct	72.1	77.0
GIN - Attr only	71.4	76.8
GIN - Attr and Struct - GCC E2E Finetuned	72.3	77.2
GIN - Attr and Struct - GCC MoCo Finetuned	72.3	77.5
GIN - Attr and Struct - SGCL E2E Finetuned	72.6	77.4
GIN - Attr and Struct - SGCL MoCo Finetuned	72.5	77.8

Table 23: Results on OGB datasets

12.3 Citeseer and Cora

We ran the frozen E2E transfer case for Citeseer and Cora datasets. When we transferred our structure-only models to these datasets and did not use any node attributes, we observed 50.8 (1.6) and 68.7 (2.1) percent accuracy on Citeseer and Cora respectively (standard deviations in brackets).

With node features included along with the frozen encoder, the performance rose to 71.5 (1.2) and 82.1 (1.6) respectively. The fact that these values (50.8 and 68.7) are significantly higher than a random guess (approx. 14.3 and 16.7) indicates that the structure-only encoder trained on a completely different pre-training corpus is still able to learn important topological characteristics.

13 Limitations, societal impact and reproducibility

Limitations. Our paper is not without limitations. Currently, the pre-train datasets we use in our paper are mostly inherited from established work focusing on GNN pre-training (Qiu et al., 2020; You et al., 2020). Even though they are sufficiently large in terms of the scale of the graph, we believe our model can be further strengthened by more diverse graph datasets. As a very recent paper GraphWorld (Palowitch et al., 2022) addressed, the commonly used datasets have graph statistics that lie in a limited and sparsely-populated region in terms of metrics such as the clustering coefficient, degree distribution, or Gini coefficient. Thus, to fully benefit from the power of pre-training techniques for graph data, it would be interesting and important to extend the use of pre-train datasets to graphs with diverse structural properties.

Another limitation of our work is that the pre-training and transfer focuses exclusively on the graph structure information; this is a common approach for cross-domain training (Qiu et al., 2020). We believe that there is value in further investigation into techniques that can process the node feature information as well as the structure information during the pre-train stage. This especially can be seen with the OGB datasets, which may share structural information between, for example, molecules and citation networks, while sharing no attribute related information.

Potential societal impact. Graph neural network techniques have been commonly used for prediction tasks in social networks and recommender systems. Our techniques, as a variant of graph neural networks, can be used in those scenarios to further improve the model performance. However, having such an ability is a double-edged sword. On one hand, it can be beneficial to improve user experience. On the other hand, if these techniques are used purely for a profit-driven or political driven reason, they can aim to 1) monopolize user attention for as long as possible by seducing users into carrying out actions that will make them happy on very short timescales and addictive to their product or even worse to 2) shape and influence public opinion on the key matters of the time. Thus, researchers and service providers should pay vigilant attention to ensure the research does end up being used positively for the social good.

Reproducibility. We have included the code and all hyperparameters, hardware details etc. to facilitate reproducibility.

14 Additional ablations

In this section, we present the variation of the model’s success with changes in train dataset, degree, the standard deviation of the degree, and λ_2 (the second eigenvalue of the Laplacian).

Table 24: Advantage of SGCL over GCC, with GCC performance in brackets, when the train set is restricted to particular graphs. The graphs are listed in descending order of their sizes.

Advantage	IMDB-M	COLLAB	RDT-B	RDT-M
All	0.5(49.3)	0.9(74.7)	0.9(87.5)	1.2(52.6)
LiveJournal	0.4 (48.8)	0.9 (74.2)	1.0 (86.9)	1.1 (51.8)
Facebook	0.5 (49.0)	0.8 (74.0)	1.0 (86.7)	1.1 (51.6)
IMDB	0.6 (48.2)	1.1 (73.8)	1.1 (86.5)	1.2 (51.5)
DBLP	0.7 (49.1)	1.1 (74.3)	1.2 (86.4)	1.1 (51.9)
Academia	0.6 (48.1)	1.0 (74.5)	1.1 (86.2)	1.1 (51.2)

In the ablations against λ_2 , degree, and standard deviation of the degree we see a pronounced U-curve where the middle quintiles perform best. This could be due to the hypothesized spectral gap effect that we derive. The results in degree statistics could well be due to the fact that such statistics in turn depend greatly on the λ_2 values, and cannot be considered truly independent findings.

Table 25: Advantage of SGCL over GCC, with GCC performance in brackets, when the train set is restricted to particular graphs. The rows represent rank quintiles of λ_2 .

Advantage	IMDB-M	COLLAB	RDT-B	RDT-M
Q1	0.3 (47.6)	0.6 (74.2)	0.8 (86.8)	0.9 (51.6)
Q2	0.3 (48.7)	0.9 (74.0)	0.8 (86.7)	1.0 (51.5)
Q3	0.7 (49.5)	1.1 (74.9)	1.2 (87.4)	1.5 (52.3)
Q4	0.9 (49.4)	1.2 (75.0)	1.2 (88.0)	1.4 (53.0)
Q5	0.3 (49.4)	0.6 (74.9)	0.7 (87.8)	1.0 (52.9)

Table 26: Advantage of SGCL over GCC, with GCC performance in brackets, when the train set is restricted to particular graphs. The rows represent rank quintiles of average degree.

Advantage	IMDB-M	COLLAB	RDT-B	RDT-M
Q1	0.4 (48.6)	0.7 (74.3)	0.8 (87.4)	1.0 (52.4)
Q2	0.5 (49.2)	0.8 (74.5)	1.0 (87.6)	1.2 (52.5)
Q3	0.6 (49.0)	1.0 (74.8)	0.9 (87.2)	1.3 (52.2)
Q4	0.5 (49.4)	1.0 (74.6)	1.0 (87.3)	1.3 (52.4)
Q5	0.6 (49.3)	1.1 (74.2)	1.0 (87.6)	1.3 (52.5)

Table 27: Advantage of SGCL over GCC, with GCC performance in brackets, when the train set is restricted to particular graphs. The rows represent rank quintiles of the standard deviation of the degree.

Advantage	IMDB-M	COLLAB	RDT-B	RDT-M
Q1	0.5 (48.4)	0.8 (74.3)	0.8 (87.2)	1.2 (52.9)
Q2	0.6 (49.5)	0.9 (74.6)	1.1 (87.6)	1.3 (52.3)
Q3	0.6 (49.6)	1.0 (75.0)	1.2 (87.6)	1.3 (52.4)
Q4	0.6 (50.0)	1.1 (75.2)	1.2 (87.7)	1.3 (52.2)
Q5	0.3 (49.0)	0.6 (74.2)	0.7 (87.5)	1.0 (52.2)

Table 28: The behavior of SGCL, E2E, Frozen on spectrally splitting a train dataset(DBLP) into 5 quintiles along the rows, according to the value of λ_2 , while testing on a similar split across the columns on COLLAB. Both diagonal and middle quintiles show elevated values.

SGCL Accuracy	Q1	Q2	Q3	Q4	Q5
Q1	73.8	73.5	73.6	73.4	73.2
Q2	73.4	73.7	73.8	73.6	73.7
Q3	73.8	74.2	74.2	74.1	74.0
Q4	73.5	73.9	74.2	74.3	73.8
Q5	73.3	73.2	73.7	73.6	73.6

15 Theorems underlying the augmentations

15.1 Crop augmentation

Let us derive a few key claims that will help us put the crop augment on a surer footing.

Denote by P_n the path-graph on n vertices, which has $n-1$ edges of form $(i, i+1)$ for $i = 1, \dots, n-1$. This corresponds to the line graph.

Define also $R_n, n \geq 3$, the ring graph on n vertices defined as P_n with an extra edge between 1 and n .

Recall the *product graph*: A product of two graphs A, B with vertex sets (v_A, v_B) and edge sets (e_A, e_B) is a graph $A.B$ where each $v \in A.B$ can be identified with an ordered pair $(i, j), i \in v_A, j \in v_B$. Two nodes corresponding to $(i, j), (i', j')$ in $A.B$ have an edge between them if and only if either $i' = i, (j, j') \in e_B$ or $(i, i') \in e_A, j = j'$. The product of two line graphs of length M, N respectively can be represented as a planar rectangular grid of lengths M, N . Denote by $G_{a,b}$ the rectangular grid graph formed by the product $P_a.P_b$. Structurally, this graph represents an image with dimensions $a \times b$.

For simplicity, we will prove our work for unweighted and undirected graphs, but the properties are general and do not require these conditions.

Theorem 2 *Let A be a graph with eigenvalues of the Laplacian as $\lambda_1, \lambda_2, \dots, \lambda_N$ and corresponding eigenvectors $\mathbf{v}_1, \dots, \mathbf{v}_N$. Similarly consider B another graph with eigenvalues μ_1, \dots, μ_M and eigenvectors $\mathbf{u}_1, \dots, \mathbf{u}_M$. Let the product of graphs A, B be C . Then, identifying each node in C with an ordered pair (x, y) , the Laplacian of C has an eigenvector \mathbf{w}_{ij} with eigenvalue $\lambda_i + \mu_j$, such that*

$$\mathbf{w}_{ij}(x, y) = \mathbf{v}_i(x) \times \mathbf{u}_j(y)$$

Proof: let the laplacian of C be L_C . We need only compute the term

$$L_C(\mathbf{w}_{ij}(x, y))$$

This is equivalent to (with e_A, e_B being the edge set of A, B respectively) :

$$\sum_{(x,x') \in e_A} (\mathbf{w}_{ij}(x, y) - \mathbf{w}_{ij}(x', y)) + \sum_{(y,y') \in e_B} (\mathbf{w}_{ij}(x, y) - \mathbf{w}_{ij}(x, y'))$$

However, taking $\sum_{(x,x') \in e_A} (\mathbf{w}_{ij}(x, y) - \mathbf{w}_{ij}(x', y))$, we observe that :

$$\sum_{(x,x') \in e_A} (\mathbf{w}_{ij}(x, y) - \mathbf{w}_{ij}(x', y))$$

becomes, applying the hypothesized $\mathbf{w}_{ij} = \mathbf{v}_i(x) \times \mathbf{u}_j(y)$

$$\sum_{(x,x') \in e_A} (\mathbf{v}_i(x)\mathbf{u}_j(y) - \mathbf{v}_i(x')\mathbf{u}_j(y))$$

Taking $\mathbf{u}_j(y)$ in common, we recognize that $\sum_{(x,x') \in e_A} \mathbf{v}_i(x) - \mathbf{v}_i(x')$ will yield just \mathbf{v}_i scaled by λ_i as \mathbf{v}_i is the eigenvector of the Laplacian.

Therefore this term becomes

$$\sum_{(x,x') \in e_A} \mathbf{u}_j(y) \times \mathbf{v}_i(x) \times \lambda_i$$

While the other term, i.e.

$$\sum_{(y,y') \in e_B} (\mathbf{w}_{ij}(x, y) - \mathbf{w}_{ij}(x, y'))$$

yields similarly

$$\sum_{(y,y') \in e_B} \mathbf{u}_j(y) \times \mathbf{v}_i(x) \times \mu_j$$

Adding the two, we see that the final matrix-vector product is parallel to the original vector (thus an eigenvector) with eigenvalue $\lambda_i + \mu_j$.

Theorem 3 *The eigenvectors of the (un-normalized) Laplacian of P_n , for $n > k \geq 0$, are of the form:*

$$\mathbf{x}_k(u) = \cos(\pi k u / n - \pi k / 2n)$$

with eigenvalues λ_k

$$2 - 2 \cos(\pi k / n)$$

Proof : We will use the ring graph defined above. Let P_n be the path graph. R_{2n+2} is clearly the ring graph obtained by having two copies of P_n with 2 additional links.

Now, R_n can be drawn on the plane with the vertex i located at $(\cos(\alpha i), \sin(\alpha i))$ where $\alpha = \frac{2\pi}{n}$. Observe that each vertex i has a position in the plane which is parallel to the sum of the position vectors of $i + 1$ and $i - 1$. From this, it naturally follows (by the definition of the Laplacian operator which subtracts the value of the neighbour vectors from that at the node) that the valid eigenvectors for R_n are :

$$\mathbf{x}_k(i) = \cos(\alpha k i), \mathbf{y}_k(i) = \sin(\alpha k i)$$

Regarding the eigenvalue, the node itself contributes 2 (as it appears in the sum twice) and each neighbour contributes $-\cos(\alpha k)$ with 2 neighbours, leading to an eigenvalue of $2 - 2 \cos(\alpha k)$.

Now it is trivial to find the eigenvectors of P_n from R_{2n} . Simply take any eigenvector of R_{2n} which has the same value for $i, i + n$ for $i \leq n$. Then the restriction of this eigenvector to $1 \leq i \leq n$ defines a valid eigenvector for P_n with the same eigenvalue. This is why the terms of the angles in the theorem are the same as path graphs with π taking the place of 2π as, for example

$$2 - 2 \cos\left(\frac{2\pi}{2n}k\right) = 2 - 2 \cos\left(\frac{\pi}{n}k\right)$$

Which is the sought result.

15.2 Reordering augmentation

Theorem 4 Let A be the adjacency matrix of an undirected unweighted graph, D the degree matrix and $P = D^{-1/2}AD^{-1/2}$ the normalized adjacency matrix. Let D_k be the k -th order normalized diffusion matrix :

$$D_k = \sum_{i=1}^k P^i$$

Then, the j -th eigenvector (sorted in order of eigenvalues and ties broken consistently) is the same for all j for any odd k . That is, for any odd k , D_k and P have eigenvectors ordered in the same sequence.

Proof : First, since the normalized Laplacian matrix L is related to P as $L = I - P$, and it has eigenvalues in the range $[0, 2]$, P has eigenvalues lying in the range $[-1, 1]$.

Now, observe that P shares the same eigenvectors with P^k for any k , however, eigenvalue λ changes to λ^k . It can be seen that since the permutation is on the basis of sorting eigenvalues, the view for $A + A^2 + \dots + A^k$ will coincide with A if $f_k(x) = x + x^2 + \dots + x^k$ is monotonic in the range $[-1, 1]$, which is the range of allowed eigenvalues of the normalized adjacency matrix. It is trivial to note that $f_k(x)$ is monotonically increasing for $x \in [0, 1]$ for any k . Now, ignoring the case $|x| = 1$, observe that $1 + f_k(x) = \frac{1-x^{k+1}}{1-x}$ by the geometric progression formula. If k is odd, $k+1$ is even, and thus x^{k+1} is positive for $x \in [-1, 0]$. As we move x from -1 to 0 the numerator monotonically rises, and the denominator monotonically falls from 2 to 1 , meaning that overall the function is monotonic and the ordering will just mirror x . This is not true when the sum terminates at an even power, for instance, $x + x^2$ which is 0 at -1 and 0 but negative at $-1/2$, indicating that it cannot be monotonic. The case where x is 1 or -1 is trivially true.

15.3 Alignment closed forms

Given a function of the following nature where Q is orthogonal

$$\|XQ - Y\|^2$$

Minimization of the above function can be done by noting that this is equivalent to working with :

$$\|XQ\|^2 + \|Y\|^2 - 2\langle XQ, Y \rangle$$

$\|XQ\| = \|X\|$, and we only have $\langle XQ, Y \rangle$ to maximize. This is $Y^T XQ$, which is equal to $\langle Q, X^T Y \rangle$. Maximizing this boils down to the projection of the matrix $X^T Y$ on the set of orthogonal matrices under the square Frobenius norm. Let the SVD of $X^T Y$ be USV^T , then we have $\langle Q, USV^T \rangle$ being maximized. This becomes $\langle U^T QV, S \rangle$, with $U^T QV$ orthogonal and made to maximize inner product with diagonal S , implying that $Q = UV^T$ is the solution.

16 Proofs on the stochastic block model

Usually, one divides graph contrastive learning and more generally all of contrastive learning into two categories :

- Supervised contrastive learning : There are unseen labels for each node. Our proofs will center on showing that with high probability, augmentations either preserve these unseen labels or some straightforward function of them that are made to suit the situation. For example, in a graph classification setting formed from the ego-graph of the nodes, the graph can be given the label of the node it is formed as an ego-graph from or the majority label of the nodes it contains. Our proofs in this case deal with the graph label and not the node label.
- Unsupervised graph contrastive learning : Each node is its own class (the classic setting of graph contrastive learning). In this scenario, it is not possible to work with the node label. Since in our setting, the nodes also possess no node-specific attributes beyond the structural information, our work here must focus on the structures obtained under spectral augmentation only.

In both cases we assume contrastive learning in general to work. That is, we show that the process of generating positive pairs etc. continues properly, but not anything about whether contrastive learning as a whole can generalize better or learn better representations. We view such a proof as outside the scope of this paper.

In the paper, we have worked with six distinct augmentations , of which two modify the structures chosen : Crop and Similar/Diverse. Three of them modify the attributes alone : Mask, reorder, and align. In general, nothing can be proven about the latter three without assuming an easy function class such as linear classifiers, which we view as unrealistic. Hence, our work focuses on the first two.

Secondly, we work with the stochastic block model and the two-cluster case where differing label of a node indicates a different propensity to create edges. We only focus on the case where there are seen or unseen labels which are related to the structure of graphs. This can be seen as a scenario intermediate between the supervised and unsupervised contrastive learning case, and the block model a natural reification to study it, for it is well known (Rohe et al., 2011) that conditional on the label of a node being known, the degree structure and density etc. strongly concentrate around their fixed values for the stochastic block model. Indeed, no other parameter except the label which directly determines the edge density even exists to provide information about the structure. Proving that nodes of similar (seen or unseen) labels are brought together by our augmentations carries over to the unsupervised case fully as these parameters are the only ones directly determining the structure.

By assuming that (unseen) labels exist, our proof is quite relevant to the actual use case of the paper. This is because in the downstream usage, the classifier is used, zero-shot, to provide representations that are used to predict the label. In other words, hidden latent labels are assumed to be predictable from the structure. Our case should be understood as a special case of unsupervised representation learning that shares some conditions with the supervised scenario.

16.1 Proof sketches and overall meaning

Our proofs center around the stochastic block model. In this setting the spectrum is well known and analyzed. We show that in this case, the “crop” operation around a node v extracts a sub-graph of nodes which largely possess the same label as v itself, where the label is considered to coincide with the cluster(block). Under the contrastive learning assumption, then, “crop” recovers positive pairs.

We also show that common embedding methods such as LINE, DeepWalk etc. are meaningful in terms of establishing “similar” and “diverse” views in the stochastic block model and that “similar” filtering would indeed yield a pathway to setting positive pairs apart. This is done by re-using our analysis for the supervised case which looks at the spectrum, and re-using the results from NETMF (Qiu et al., 2018) which connects the spectral results to embeddings obtained by random walks. In short, random walks and corresponding embeddings on stochastic block models can be seen, in the limit, as spectral decompositions of a block model with parameters that depend on the original block model. After this, we can recognize that the analysis for “crop”, which essentially shows that the spectral embeddings form a meaningful metric of closeness in terms of label, cluster etc. on the original model, fully carries over with transformed parameters.

16.2 Supervised contrastive learning derivation

We define our stochastic block model (Rohe et al., 2011) as follows in keeping with conventions of the field. We will consider one with two components.

- There are N_0 nodes generated with label 0, and N_1 with label 1. Denote the group generated with label 0 as C_0 and the other as C_1 . For simplicity, set $N_0 = N_1 = N$
- An edge occurs with probability p among two nodes of label 0, with probability q between two nodes of label 1, and with z among two nodes of different labels. $z < \min(p, q)$ is a common assumption. Without loss of generality we can take $p > q > z$. We also consider the self-edges to be valid.

Note that in the setting of GCC, different local structures encode different labels. Hence $p \neq q$, as if they were equal it would imply the same structural generation process gives rise to two different labels.

Let A be the adjacency matrix of the stochastic block model and L the laplacian. Let $\lambda_n(v)$ be the function that assigns to a node v its value under the n -th eigenvector of the Laplacian. Let $C_\epsilon(v)$ be the cropped local neighbourhood around any node v defined as $\{v' : \|\lambda(v') - \lambda(v)\| \leq \epsilon\}$ where $\lambda(v) = [\lambda_2(v), \lambda_3(v)]$.

16.3 Factorizing the adjacency matrix

The overall matrix A is of shape $2N \times 2N$. Recall that we have allowed self-edges and diagonal entries of A are not zero. Consider the matrix :

$$\begin{bmatrix} p & z \\ z & q \end{bmatrix}$$

Let W be a $2N \times 2$ matrix formed by repeating the row vector $[1 \ 0]$ N times and then the row vector $[0 \ 1]$ N times. W denotes the membership matrix. The first N rows of W denote that first N nodes belong to label 0 (and hence their zero-th entry is 1) and the next N rows likewise have a 1 on their 2-nd column signifying that they have label 1.

Now, we can see that if we multiply $W \begin{bmatrix} p & z \\ z & q \end{bmatrix}$, the first N rows of the resulting $2N \times 2$ matrix will be $[p \ z]$ and the next N will be $[z \ q]$. Consider now multiplying from the right side with W^T i.e. forming, overall, $W \begin{bmatrix} p & z \\ z & q \end{bmatrix} W^T$. This matrix will be of shape $2N \times 2N$ and it can be seen that it has a block structure of form :

$$\begin{bmatrix} p(1_N 1_N^T) & z(1_N 1_N^T) \\ z(1_N 1_N^T) & q(1_N 1_N^T) \end{bmatrix}$$

Where, 1_N is the $N \times 1$ vector of all 1-s, and $1_N 1_N^T$ the $N \times N$ matrix of all 1-s. So, it can be seen that the above matrix is nothing but the expectation of the stochastic block model's adjacency matrix.

Now, can we avoid analyzing this matrix and instead settle for analyzing the comparatively simpler $\begin{bmatrix} p & z \\ z & q \end{bmatrix}$? Let v be an eigenvector of $\begin{bmatrix} p & z \\ z & q \end{bmatrix}$ with eigenvalue λ . Let v have entries $\begin{bmatrix} x \\ y \end{bmatrix}$. By hypothesis, $\begin{bmatrix} p & z \\ z & q \end{bmatrix} v = \lambda v$. Then, if we have the vector v' of shape $2N \times 1$ with first N entries as x , and the next N as y

$$\begin{bmatrix} p(1_N 1_N^T) & z(1_N 1_N^T) \\ z(1_N 1_N^T) & q(1_N 1_N^T) \end{bmatrix} v' = (\lambda N) v'$$

It can be seen that v' is parallel to an eigenvector of the expectation of the adjacency matrix and the corresponding eigenvalue is λN . However, we always assume eigenvectors are of unit norm, i.e. $x^2 + y^2 = 1$. So, v' is going to be not x repeated N times, but $\frac{x}{\sqrt{N}}$ N times and then $\frac{y}{\sqrt{N}}$ N times. This makes $\|v'\| = 1 = \|v\|$. Therefore, for every pair λ, v in the spectra of the 2×2 matrix, there is a corresponding $\lambda N, v'$ in the spectra of the expectation of the adjacency matrix. Next, note that

the rank of the expectation of the adjacency is $\leq \text{Rank}\begin{pmatrix} p & z \\ z & q \end{pmatrix} \leq 2$. So if the 2×2 matrix has a full rank, there can be no extra eigenvalue-eigenvector pairs for the corresponding expectation of the adjacency matrix. All the nonzero eigenvalues and corresponding eigenvectors of the expectation of the adjacency are derivable from the 2×2 matrix's spectra. **In short, to understand the spectrum of the expectation of adjacency, we can just study the 2×2 matrix, as there is a one to one relationship between the nonzero eigenvalues and corresponding eigenvectors.**

16.4 Crop augmentation

Notation of probability. In proofs involving convergence, it is customary to provide a guarantee that a statement holds with probability $\geq 1 - F(N)$ where $F(N)$ tends to zero as N goes to infinity. We will somewhat abuse the notation and say the probability $\rightarrow 1$ as $N \rightarrow \infty$ to denote this. We do not distinguish between things such as convergence in probability, convergence in distribution, almost surely convergence etc. and provide a largely concentration-inequality based proof overview.

We can state our proof for the **crop augmentation** as follows. All of the following statements hold with high probability (i.e. hold with a probability that $\rightarrow 1$ as $N \rightarrow \infty$.)

Theorem 5 *Let the number of samples $N \rightarrow \infty$. Let v be chosen uniformly at random from the nodes. The following statements hold with a probability that $\rightarrow 1$ as $N \rightarrow \infty$:*

- **Proposition 1** : *The majority label in $C_\epsilon(v)$ is the label of v .*
- **Proposition 2** : *Two nodes v, v' of different labels generate non-isomorphic cropped subgraphs $C_\epsilon(v), C_\epsilon(v')$, if v' is chosen uniformly at random as well.*
- **Proposition 3** : *For any v and $C_\epsilon(v)$, there is no differently labeled v' and $C_\epsilon(v')$ which is isomorphic to $C_\epsilon(v)$ for a high enough ϵ , if both are chosen uniformly at random.*

Note that in the main text, we state a slightly different version of the theorem (Theorem 1 of the main text) involving ego networks as well, which we restate here :

Theorem 6 *Let node v be chosen uniformly at random from G , a $2N$ -node graph generated according to the SBM described above. With probability $\geq 1 - f(N)$ for a function $f(N) \rightarrow 0$ as $N \rightarrow \infty$, $\exists \epsilon \in \mathbb{R}^+, k_{max} \in \mathbb{N}$ such that :*

$$\forall k \in \mathbb{N} \leq k_{max}, Y(E_{k,v}(G)) = Y(C_\epsilon(v)) = Y(v) \quad (7)$$

Terming k_{max} used above as k_{crit} , we can see that this is adding an extra part that agrees with the node label, namely the majority label of an ego network. However, the majority label for the k ego network when $k \leq k_{crit}$ is trivially equal to the node's label for at least some values of k_{crit} allowing k beyond 0 (i.e. the node itself is the ego network). To see this, take $k = k_{crit} = 1$. The expected number of nodes of the same label - considering label 0 for simplicity - in its ego network is $p(N - 1) + 1$, and the ones of a different label are of expected number zN . By Hoeffding's inequality, both quantities with high probability i.e. with probability $\geq 1 - O(\exp(-\delta^2))$ have deviations of only $O(\delta\sqrt{N})$ from their expectations which are terms of $O(N)$. Therefore, the majority label agrees with the node's own label with high probability (note that this requires $p, q > z$). We assume this step to hold with high probability and focus now on proving the equality of the cropped subgraph's majority label and the node label. We discuss ego networks other than the 1-ego network at the end of the section. It can be easily checked that at least for the 1-ego network, our proof involving mostly the vertex label case requires no changes.

To prove this, consider the random matrix A . We can denote the expectation of A as A^* . We can see the rank of A^* is 2 as it has exactly 2 possible types of columns in it. It remains to find the corresponding two eigenvectors and eigenvalues. Clearly, by the structure of the matrix, the eigenvectors are of the form of repeating one value c N times and then another value c' N times, and we can WLOG set $c = 1$ and replace c' with c . Then it remains to solve

$$\begin{bmatrix} p & z \\ z & q \end{bmatrix} \begin{bmatrix} 1 \\ c \end{bmatrix}$$

Which becomes, by the definition of eigenvector,

$$\frac{z + qc}{p + zc} = c$$

or, simplifying :

$$zc^2 + (p - q)c - z = 0$$

Therefore, by the quadratic formula :

$$c = \frac{(q - p) \pm \sqrt{(p - q)^2 + 4z^2}}{2z}$$

The eigenvalue for a corresponding c is $p + zc$. Since $p, z \geq 0$ the larger eigenvalue λ_1 corresponds always to the larger value of c . Therefore, λ_2 takes the value gained by plugging in the negative root above, for c . This yields the **unnormalized** eigenvector, the actual entries assigned under the eigendecomposition are respectively $\frac{1}{\sqrt{1+c^2}}, \frac{c}{\sqrt{1+c^2}}$ when a vertex v is assigned its value under the eigenvector.

We re-use previous results in random matrix theory (Vu, 2007) (theorem 1.4) that imply that with a probability $\rightarrow 1$, $\|A - A^*\|_{op} \leq \sqrt{18pN}$, when p is $\Omega(\log N)^4/N$. Since the lower bound on $p \rightarrow 0$ as $N \rightarrow \infty$ we can assume it to hold for large N . The $\|\cdot\|_{op}$ notation denotes operator norm.

Explanation of the order through Hoeffding and RIP property. To intuitively understand the above result, we can consider each entry of $A - A^*$. This is a random variable (blockwise) that takes one among the following set of values : $-p, 1 - p$ (among the $N \times N$ entries of label 0), $-z, 1 - z$ (among the $2 \times N \times N$ entries between labels 0, 1) and $-q, 1 - q$ (among label 1). Now, only the upper triangle and diagonal are independent as the edges are symmetric, and the matrix is symmetric about the diagonal. We can write that :

$$\|A - A^*\|_F^2 = 2\|A - A^*\|_{F,UT}^2 + \|A - A^*\|_{F,D}^2$$

Where, F denotes Frobenius norm, and UT, D respectively denote summing over upper triangular and diagonal indices.

Therefore, if each entry of $A - A^*$ be denoted as Δ_i , enumerated in any order over the diagonal and upper triangle of the $2N \times 2N$ matrix ($1 \leq i \leq N(2N + 1)$), Δ_i, Δ_j are independent r.v.s for any $i \neq j$. Further, $-1 \leq \Delta_i \leq 1$. Therefore, $0 \leq \Delta_i^2 \leq 1$. Further, $\|A - A^*\|_F^2 \leq \sum 2\Delta_i^2$.

$\sum \Delta_i^2$ is a sum of independent random variables in a fixed, finite range of size 1. Therefore, Hoeffding's inequality applies, which yields that with probability $\geq 1 - O(1/N)$:

$$E\left(\sum \Delta_i^2\right) - \sqrt{N(N + 1/2) \log(N)} \leq \sum \Delta_i^2 \leq E\left(\sum \Delta_i^2\right) + \sqrt{N(N + 1/2) \log(N)}$$

$E(\sum \Delta_i^2)$ is the sum of the variances of random variables Δ_i over $N(2N + 1)$ entries, bounded above by 1. Hence, it follows that $\|A - A^*\|_F^2$ is $O(N^2)$ with probability $\geq 1 - O(1/N)$, therefore, $\|A - A^*\|_F$ is $O(N)$.

Further, we can see that $A - A^*$ has the following structure :

$$\begin{bmatrix} J & K \\ K & L \end{bmatrix}$$

Where, J, L are symmetric matrices with each upper triangular and diagonal entry as i.i.d random variables Z satisfying :

$$Z = a \text{ with probability } p \text{ else } Z = b, E(Z) = 0$$

In addition, K is a matrix (not necessarily symmetric) which has every entry as i.i.d realizations of such Z . Then, such a matrix $\begin{bmatrix} J & K \\ K & L \end{bmatrix}$ by Restricted Isometry Property (Vu, 2014) has the property that, with high probability, there is a constant K' independent of N :

$$\max_i \lambda_i(A - A^*) \approx \sqrt{\frac{K'}{N} \sum_{i=1}^N \lambda_i^2[(A - A^*)]}$$

The left hand side is the maximum eigenvalue, which we recognize as $\|A - A^*\|_{op}$ i.e. the operator norm.

Now, using the relation between eigenvalues and the Frobenius norm :

$$\sum_{i=1}^N \lambda_i^2[(A - A^*)] = \|A - A^*\|_F^2 = O(N^2)$$

The RHS comes from plugging in the Frobenius norm bound from the Hoeffding's inequality step. Finally, this yields :

$$\|A - A^*\|_{op} = O(\sqrt{N})$$

The result of Vu's we state above is merely a formalization of this sketch with constants, the order is the same i.e. \sqrt{N} .

Now consider the second eigenvector i.e. the λ_2 function from A against the calculated λ_2 above for A^* . We need to use the Davis Kahan theorem (Demmel, 1997) (theorem 5.4) which states that if the angle between these is θ , then

$$\sin 2\theta \leq \frac{2\|A - A^*\|_{op}}{2N * \min(|\mu_1 - \mu_2|, \mu_2)}$$

As both eigenvectors are unit vectors, we can use the property that if two unit vectors have angle θ between them, the norm of their difference is bounded above by $\sqrt{2}\sin\theta$. Ignoring constants, we end up with the result that for some constant c_0 , and denoting $v_{M,i}$ the i -th eigenvector of the Laplacian formed from some adjacency matrix M

$$\|v_{A,2} - v_{A^*,2}\| \leq c_0 \frac{\sqrt{pN}}{N * \min(|\mu_1 - \mu_2|, \mu_2)}$$

The LHS however works with the eigenvector of the overall adjacency matrix formed by the multiplication by W we have discussed above. Recall that we have already noted the adjacency matrix and the 2×2 matrix share eigenvalues upto scaling in N . Their eigenvectors are also likewise related, and since eigenvectors are always of unit norm, an eigenvector of the 2×2 matrix is first repeated in its entries and then normalized by a factor of $\frac{1}{\sqrt{N}}$ by virtue of being an eigenvector, to become an eigenvector of the overall adjacency matrix.

By substituting the eigenvectors we found earlier, i.e. $\frac{1}{\sqrt{1+c^2}}[1, c]^T$ into the LHS, scaling by this \sqrt{N} factor cancels the extra \sqrt{N} on the RHS. Recalling that

$$c = q_1 = \frac{(q-p) - \sqrt{(p-q)^2 + 4z^2}}{2z}$$

Let :

$$S_1 : \{x : v_{A^*,2}(x) = \frac{1}{\sqrt{1+q_1^2}}, v_{A,2}(x) \leq \frac{1+q_1}{2\sqrt{1+q_1^2}} + \frac{\epsilon}{2}\}$$

$$S_2 : \{x : v_{A^*,2}(x) = \frac{q_1}{\sqrt{1+q_1^2}}, v_{A,2}(x) \geq \frac{1+q_1}{2\sqrt{1+q_1^2}} - \frac{\epsilon}{2}\}$$

Let v_1, v_2 be any pair of nodes that satisfy the conditions of :

- Labels of v_1, v_2 are different. WLOG, let v_1 have label 0, v_2 label 1.

- $C_\epsilon(v_1)$ contains v_2 (and by symmetry, $C_\epsilon(v_2)$ contains v_1)

Clearly, we can see that either $v_1 \in S_1$ or $v_2 \in S_2$. Let $K_1 = |S_1|, K_2 = |S_2|$. Summing only over S_1 :

$$K \left(\frac{1 - q_1}{2\sqrt{1 + q_1^2}} - \epsilon/2 \right)^2 \leq \frac{p(c_0)^2}{\min((\mu_1 - \mu_2)^2, \mu_2^2)}$$

This yields a bound on K_1 , which we can term $K_{1,max} = \frac{p(c_0)^2}{\left(\frac{1 - q_1}{2\sqrt{1 + q_1^2}} - \epsilon/2\right)^2 \times \min((\mu_1 - \mu_2)^2, \mu_2^2)}$. Similarly, we can consider K_2 to get $K_{2,max}$ as : $\frac{p(c_0)^2}{\left(\frac{1 - q_1}{2\sqrt{1 + q_1^2}} - \epsilon/2\right)^2 \times \min((\mu_1 - \mu_2)^2, \mu_2^2)}$. Set $\epsilon = \frac{1 - q_1}{2\sqrt{1 + q_1^2}}$ to get :

$$K_{1,max} + K_{2,max} \leq \frac{2p(c_0)^2}{\left(\frac{1 - q_1}{4\sqrt{1 + q_1^2}}\right)^2 \times \min((\mu_1 - \mu_2)^2, \mu_2^2)}$$

Since $K_{1,max} = K_{2,max}$ we can term it K_{max} . Simultaneously, consider :

$$S_3 : \left\{ x : v_{A^*,2}(x) = \frac{1}{\sqrt{1 + q_1^2}}, v_{A,2}(x) \geq \frac{1 + q_1}{2\sqrt{1 + q_1^2}} + \frac{3\epsilon}{2} \right\}, \epsilon = \frac{1 - q_1}{2\sqrt{1 + q_1^2}}$$

$$\frac{1 + q_1}{2\sqrt{1 + q_1^2}} + \frac{3\epsilon}{2} = \frac{\frac{5}{4} - \frac{q_1}{4}}{\sqrt{1 + q_1^2}} \geq \frac{1}{\sqrt{1 + q_1^2}} + \frac{1}{4\sqrt{1 + q_1^2}}$$

Last inequality is by the property $q_1 < 0$. By a similar argument as for S_1, S_2 , S_3 is of constant size and $\frac{S_3}{N} \rightarrow 0$ as $N \rightarrow \infty$. Let the maximum size of S_3 be $K_{3,max}$. Now, if we pick a vertex v of label 0 at random, with probability $\geq 1 - \frac{K_{3,max} + K_{max}}{N}$, $v \notin S_1, v \notin S_3$. If both these conditions hold, in $C_\epsilon(v)$ any v' which does not have the same label must have $v' \in S_2$. (Because any such pair must have at least one element in S_1, S_2 and $v \notin S_1$). Simultaneously, $C_\epsilon(v)$ contains at least all vertices of label 0 not in $S_1 \cup S_3$ i.e. has vertices of label 0 $\geq N - K_{3,max} - K_{max}$. Noting that K values are all constants and $N \rightarrow \infty$ implies that majority label in $C_\epsilon(v)$ will agree with v as $K_{max}/N \rightarrow 0$ completes the proof. The only aspect of the proof which required high probability was the norm of $\|A - A^*\|_{op}$ varying as \sqrt{N} , this step may be assumed to be true with probability $\geq 1 - O(1/N^3)$ (tighter bounds are possible but this suffices). **This concludes the proof of proposition 1.**

Tightness of operator norm. Consider the statement that :

$$\|A - A^*\|_F^2 = O(N^2)$$

Recall that we showed :

$$E\left(\sum \Delta_i^2\right) - \sqrt{N(N + 1/2) \log(N)} \leq \sum \Delta_i^2 \leq E\left(\sum \Delta_i^2\right) + \sqrt{N(N + 1/2) \log(N)}$$

With high probability. We used the bound of the RHS, but the bound of the LHS is also true. Hence, $\|A - A^*\|_F^2 = \Theta(N^2)$.

Next, we used :

$$\max_i \lambda_i(A - A^*) \approx \sqrt{\frac{K'}{N} \sum_{i=1}^N \lambda_i^2[(A - A^*)]}$$

However :

$$\max_i \lambda_i(A - A^*) \geq \sqrt{\frac{1}{N} \sum_{i=1}^N \lambda_i^2[(A - A^*)]}$$

Therefore, $\max_i \lambda_i(A - A^*) = \|A - A^*\|_{op} = O(\sqrt{N})$.

In short, every step till we apply the Davis-Kahan bound, i.e. :

$$\|v_{A,2} - v_{A^*,2}\| \leq c_0 \frac{\sqrt{pN}}{N * \min(|\mu_1 - \mu_2|, \mu_2)}$$

Is as tight as possible.

Tightness of Davis-Kahan bound. The Davis-Kahan upper bound is sharp. That is, $\exists S, H, S = S^T, H = H^T$, with $\mu_1 \geq \mu_2 \geq \dots \mu_N$ the eigenvalues of S , v_1, v_2, \dots, v_N the corresponding eigenvectors of S , v'_1, v'_2, \dots, v'_N the eigenvectors of $S + H$, θ_i the angle between v_i, v'_i satisfying :

$$\sin(2\theta_i) = c' \frac{2\|H\|_{op}}{\min_{j \neq i} |\mu_i - \mu_j|}$$

Where c' is a constant ≤ 1 that does not depend on N . And at the same time, $\forall S, H, \mu_i, v_i, v'_i$:

$$\sin(2\theta_i) \leq \frac{2\|H\|_{op}}{\min_{j \neq i} |\mu_i - \mu_j|}$$

However, in our case, S is not arbitrary, but $S = A^*$. When we take $\exists S$, it allows taking e.g. $S = \begin{bmatrix} 0.6 & 0.8 \\ 0.8 & 0.7 \end{bmatrix}$. But this cannot be A^* with $N = 1$, as it violates all our assumptions for A^* , here $p = 0.6, q = 0.7, z = 0.8$ violating $p > q > z$ assumptions. We need to show that $\exists S, N, H$ such that $H = H^T$ and :

$$S = W S' W^T, S' = \begin{bmatrix} p & z \\ z & q \end{bmatrix}, 0 \leq z \leq q \leq p \leq 1$$

with W of shape $2N \times 2$ such that first N rows of W are $[1, 0]$, next N are $[1, 0]$. This makes $S = S^T$ and we already constrain $H = H^T$. With $\mu_1 \geq \mu_2 \geq \dots \mu_{2N}$ as eigenvalues of S , $v_1, v_2, \dots, v_{2N}, v'_1, v'_2, \dots, v'_{2N}$ corresponding eigenvectors of $S, S + H$ we must show $\exists i$

$$\sin(2\theta_i) = c'' \frac{2\|H\|_{op}}{\min_{j \neq i} |\mu_i - \mu_j|}$$

Where c'' is constant, not a function of N . This is reached at :

$$S' = \begin{bmatrix} 0.6 & 0 \\ 0 & 0.4 \end{bmatrix}, H' = \begin{bmatrix} -0.1 & 0.1 \\ 0.1 & 0.1 \end{bmatrix}$$

$$S = W S' W^T, H = W H' W^T$$

Where W is as specified and of shape $2N \times 2$.

Proof of proposition two.

Recall that by the proof of proposition one, $C_\epsilon(v)$ contains M nodes of label 0, where if v is selected randomly over all nodes with label 0, with probability $\rightarrow 1, \frac{M}{N} \rightarrow 1$. This step is with probability $\geq 1 - O(1/N^3)$.

Let E_0 be the set of all edges (v_i, v_j) with v_i, v_j having label both labels 0. Let $M(0, v)$ be the set of all edges (v_i, v_j) s.t. $(v_i, v_j) \in E_0, v_i, v_j \in C_\epsilon(v)$. Clearly, $M_{0,v} \subseteq E_0$, and since $\frac{M}{N} \rightarrow 1, \frac{|M_{0,v}|}{|E_0|} \rightarrow 1$.

By a similar argument, let $M_{1,v'}, E_1$ be the corresponding edge sets for $C_\epsilon(v')$ with label of v' being 1, $\frac{|M_{1,v'}|}{|E_1|} \rightarrow 1$.

E_0, E_1 are, denoting $B_w(p)$ as an independent Bernoulli random variable of bias p :

$$E_0 = \sum_{w=1}^{N(N+1)/2} B_w(p), E_1 = \sum_{w=1}^{N(N+1)/2} B_w(q)$$

Via Hoeffding's inequality, $E_0 = (pN(N+1)/2) + O(N\sqrt{\log N})$, $E_1 = (qN(N+1)/2) + O(N\sqrt{\log N})$ with probability $\geq 1 - O(1/N^3)$. Therefore, with probability $\geq 1 - O(1/N^3)$, $C_\epsilon(v), C_\epsilon(v')$ are not isomorphic. **This proves proposition two.** Applying the union bound over all choices of (v, v') **proves proposition three**, because number of possible pairs is $O(N^2)$ and the property holds with $\geq 1 - O(1/N^3)$, leading to overall probability $\geq 1 - O(1/N)$.

Note that the step of the 1 ego-network's majority label agreeing with the node's label was derived by Hoeffding's inequality and does not affect any order used so far. **Hence, this completes the proof of propositions 1, 2, 3.**

16.5 Embedding-based similarity

First, we remind the reader that usually, each node embedding method such as LINE (Tang et al., 2015) always normalizes its embedding per node. That is, each node v receives some vector e_v with $\|e_v\| = 1$. But that, in turn implies that given two distinct embeddings $e_v, e_{v'}$,

$$\frac{\langle e_v, e_{v'} \rangle}{\|e_v\| \|e_{v'}\|} = \langle e_v, e_{v'} \rangle$$

$$\|e_v - e_{v'}\|^2 = \|e_v\|^2 + \|e_{v'}\|^2 - 2\langle e_v, e_{v'} \rangle = 2 - 2\langle e_v, e_{v'} \rangle$$

That is, selecting on the more similar cosine distance (similar filtering) is equivalent to selecting on lower values of $\|e_v - e_{v'}\|$ - the type of proximity analyzed in crop. This simplifies our analysis, allowing re-use of crop results.

In the context of embeddings, let us analyze two in particular : DeepWalk (Perozzi et al., 2014) and LINE (Tang et al., 2015). It is known previously from the analysis of NETMF (Qiu et al., 2018) that these methods replicate matrix factorization. Specifically, let A, D be the adjacency matrices and degree matrices, then :

$$P_r = \frac{1}{T} \left(\sum_{r=1}^T (D^{-1}A)^r \right) D^{-1}$$

Let the volume of a graph G $V(G)$ be the sum of the number of edges, then $\log(V(G)P_r) - \log b$ where b is the negative sampling rate is a matrix Z_r . Under the framing above, DeepWalk factors any Z_r , while LINE factors Z_1 , i.e. LINE is a special case of DeepWalk. This log is taken per element.

Now, we are ready to state our theorems for similarity. Let $E(v)$ be the embedding assigned to a node v . Let p, q, z be as before.

Theorem 7 *Let the number of samples $N \rightarrow \infty$, $\frac{p}{q} \neq \infty$, $\exists \epsilon_{crit}$ such that $\forall v$, let $\{S_v : v', \text{label}(v') = \text{label}(v), \|E(v) - E(v')\| \leq \epsilon_{crit}\}$, then, $\frac{|S_v|}{N} \rightarrow 1$ and $C_{\epsilon_{crit}}(v)$ satisfies the three propositions of theorem 1, when v is chosen uniformly at random.*

Our proof for this will first translate the graph adjacency to familiar matrix forms. Note that $V(G)$ is equal to, in expectation and allowing self-loops, as :

$$2N^2(p/2 + q/2 + z)$$

Further, we can set $b = 1$ to remove it from consideration. Set $r = 1$ to recreate the case of LINE. Now, by a similar argument as for the cropping analysis for SBM where the matrix W generates the A^* matrix using a 2×2 matrix, we can examine the 2×2 matrix which is :

$$\begin{bmatrix} \frac{p}{(p+z)^2} & \frac{z}{(p+z)(q+z)} \\ \frac{z}{(p+z)(q+z)} & \frac{q}{(q+z)^2} \end{bmatrix}$$

Now, let us apply the logarithm to get our new values of p', q', z' which will be fed back to crop analysis and behave equivalently to the original parameters (as before in the crop case, the N^2 term in $V(G)$ can be ignored while reducing to the 2×2 case) :

$$p' = \log p - 2 \log(p + z) + \log(p + q + 2z)$$

$$q' = \log q - 2 \log(q + z) + \log(p + q + 2z)$$

$$z' = \log z - \log(p + z) - \log(q + z) + \log(p + q + 2z)$$

Note that $p > q$ implies $p' < q'$, as :

$$p' - q' = \log p - \log q + 2 \log(q + z) - 2 \log(p + z)$$

$$p(q + z)^2 - q(p + z)^2 = pq^2 + pz^2 - qp^2 - qz^2 = (p - q)(z^2 - pq) < 0$$

And, $p > z$ implies $p' > z'$, as :

$$p' - z' = \log p - \log(p + z) + \log(q + z) - \log z$$

$$p(q + z) - z(p + z) = pq - z^2 > 0$$

Therefore, the analysis from the crop case carries over, except we swap the order of p, q . This is equivalent to swapping the labels of the nodes, and makes no difference. Recall that the error rate for the spectral analysis in the crop section depends on p' (numerator) and $\min(\mu_2, |\mu_1 - \mu_2|)$ (denominator) \implies : the error will remain bounded above iff : $|p'|, |q'|$ are bounded above and $\min(\mu_2, |\mu_1 - \mu_2|)$ are bounded below.

Cases of issues in p', q' . Can be ruled out as follows :

- $p' = \log p - 2 \log(p + z) + \log(p + q + 2z) \leq \log p - 2 \log p + \log 4p = \log 4$.
- $q' \leq \log q - 2 \log q + \log(4p) = \log 4 + \log(p/q) < \infty$ by hypothesis $p/q \neq \infty$.

Case of eigenvalue issues, i.e. : $\min(\mu_2, |\mu_1 - \mu_2|) \rightarrow 0 \implies \mu_2 \rightarrow 0, \mu_1 - \mu_2 \rightarrow 0$. From the analysis of crop, the eigenvalues are of the form $p' + z'c'$ where :

$$c' = \frac{(q' - p') \pm \sqrt{(p' - q')^2 + 4z'^2}}{2z'}$$

Note that z' is < 0 . To see this, observe that :

$$(p + q + 2z)z = 2z^2 + pz + qz = (p + z)(q + z) - pq + z^2 < (p + z)(q + z)$$

Simultaneously, $p' > 0$, as :

$$p(p + q + 2z) - (p + z)^2 = pq - z^2$$

So the eigenvalues are :

$$\mu_1 = \frac{(q' + p') + \sqrt{(p' - q')^2 + 4z'^2}}{2}, \mu_2 = \frac{(q' + p') - \sqrt{(p' - q')^2 + 4z'^2}}{2}$$

$$\min \mu_2, |\mu_2 - \mu_1| = 0 \iff z' \rightarrow 0$$

$$0 > z' = \log(pz + qz + 2z^2) - \log(pq + pz + qz + z^2) = \log\left(1 - \frac{pq - z^2}{pq + z^2 + pz + qz}\right)$$

Since $p > q > z$, $pq - z^2 > 0$, $z' \rightarrow 0$ is not possible, and we are done. We simply need to adjust for the final step of vertex-wise normalization. Since in this case, μ_1 and its corresponding eigenvector is also utilized, we have that all elements of cluster 0 receive embeddings of form (recall q_1, q_2 are the roots of the quadratic for c) $[\frac{1}{\sqrt{N(1+q_1^2)}}, \frac{1}{\sqrt{N(1+q_2^2)}}]$ pre-normalization, and upon vertex-wise normalization this becomes $[\frac{\sqrt{1+q_2^2}}{\sqrt{2+q_1^2+q_2^2}}, \frac{\sqrt{1+q_1^2}}{\sqrt{2+q_1^2+q_2^2}}]$. For cluster 2, the corresponding post-normalization embeddings are $[\frac{q_1\sqrt{1+q_2^2}}{\sqrt{q_1^2+q_2^2+2q_1^2q_2^2}}, \frac{q_2\sqrt{1+q_1^2}}{\sqrt{q_1^2+q_2^2+2q_1^2q_2^2}}]$. These are both on expectation and all the gaps in expectation remain $O(N)$ with deviations of $O(\sqrt{N})$. Re-applying the results from the crop section, we get that there is ϵ_{crit} such that with probability $\geq 1 - O(1/N^3)$ with a fixed v , a fraction $v' \rightarrow 1$ sharing the label of v lies within ϵ_{crit} , while at most $O(1)$ (the K_{max} terms derived earlier) do not fall within this ϵ_{crit} or are v'' not sharing the label of v but lying within ϵ_{crit} . Most importantly, q_1, q_2 differ in sign, making the inner product consist of two positive terms between nodes of same label with high probability and one positive and one negative term between nodes of differing labels - the inner product is now a meaningful similarity metric ! For an easy example, we can see that setting $p = q$ leads to (in expectation) embeddings $[\frac{1}{\sqrt{2}}, \frac{1}{\sqrt{2}}]$ for one label/cluster and $[\frac{1}{\sqrt{2}}, \frac{-1}{\sqrt{2}}]$ for the other. This means nodes of two differing labels have ≈ 0 inner product and two of the same have inner product ≈ 1 with high probability.

Clearly, in the SBM case, **similar filtering** is the correct course of action with the threshold being this ϵ_{crit} . It is plausible that in other generative graph cases, this would not be the case. However, in our experiments, **similar** was always superior to diverse filtering, possibly reflecting that real life graphs are well-modeled by SBMs in this aspect. Note also that our graphs such as LiveJournal, FaceBook etc. arrive from communities in social networks which may be expected to display a clustered / stochastic block model type of pattern. Note that the factorization under the transformed parameters is not necessarily a descending algebraic decomposition, but one where we perform the decomposition in order of magnitude.

16.6 Ignorable perturbation effect from third eigenvector

In both the proofs, we have examined only 2-component SBMs. In these cases, μ_3 and its corresponding eigenvector plays no role and indeed we have proven everything in terms of μ_2, λ_2 alone. This is because in the expected adjacency matrix, $\mu_3 = 0$.

The proof fully extends to the case where λ_3 is added. For simplicity, we did not add it, and the only change required is that for every node, we instead use $\mu_2\lambda_2$ instead of λ_2 , and $\mu_3\lambda_3$ instead of λ_3 . Since μ_3 in the original expected adjacency (A^*) is zero, it is solely from $A - A^*$ that μ_3 arises. By Weyl's eigenvalue perturbation theorem (Weyl, 1912),

$$\lambda_3(A - A^*) \leq \mu_3 \leq \lambda_1(A - A^*)$$

We know, however, that $A - A^*$ is a RIP matrix (Vu, 2014) and thus $\mu_3 \approx \sqrt{N}$. This is with respect to the full matrix, i.e. $W \begin{bmatrix} p & z \\ z & q \end{bmatrix} W^T$ being A . This has μ_2 as $O(N)$, making μ_3 and thus $\mu_3 v_3$ only $\frac{1}{\sqrt{N}}$ relative to the other terms, and thus ignorable in the final embedding.

16.7 The case of DeepWalk

We sketch here the proof extension of the LINE case to DeepWalk. In DeepWalk, the matrix $D^{-1}A$ is replaced with the average over the first T powers, that is :

$$\frac{1}{T} \sum_{r=1}^T (D^{-1}A)^r$$

First note a few things. A is the adjacency matrix which we know to be of form (in expectation) as WBW^T where B is 2×2 . A^2 is $WBW^T WBW^T$. But, $W^T W$ is a scaled identity matrix. Thus A^2 in expectation is WB^2W^T (times factors purely in N). Ergo, the analysis can still be carried out in terms of B , only this time using B^2 . Next, note that replacing A with any sum of powers of K does not change the eigenvectors, it only changes the eigenvalues, because :

$$M = USU^T \rightarrow M + M^2 \dots M^K = U(S + S^2 \dots + S^K)U^T$$

The final right multiplication with D^{-1} does not affect this conclusion, since right multiplication with any diagonal matrix simply changes eigenvectors by inverse of the said matrix. Since the eigenvectors remain the same, all the steps crop onward to filtering continue to function, but the scaling factors might change due to eigenvalue changes. Since the eigenvalue change does not change finitely large quantities to infinitely small quantities and we only use this step to rule out noise from the third eigenvector, which after normalization contributes a term of order $O(\frac{1}{\sqrt{N}})$ relative to the other terms, all the steps continue to work.

Caveats and extensions. In the following subsections, we check some alternate scenarios of other ways to do NETMF, ≥ 3 components, and most importantly how random walk augmentations and ego networks of distances ≥ 2 may shift our analysis. These subsections should be considered as extensions of the main proof and mostly expository.

16.8 NETMF rounding vs no rounding.

In the NETMF implementation, terms < 1 before taking the log can be rounded up to 1 in an alternate usage. This case either results in no off diagonal entries after the log (making the analysis trivial as it is the adjacency matrix of two disconnected blocks) or a zero matrix making it nonsensical. Thus, we did not analyze this case, as in this case our augmentations either trivially work or no sensible embedding is produced at all due to a matrix of all zeroes.

16.9 Extension to 3 and greater components

In the cases of ≥ 3 component SBMs, the eigenvectors are significantly more complicated than for a 2×2 case. However, the consistency of spectral clustering under the L_2 norm - which is, as one might recognize, what we have shown here with some modifications - is proven in alternate ways, and convergence is guaranteed so long as the number of eigenvectors used is k and equal to the number of components. However, these proofs carry over to the case where the eigenvalues after 3 satisfy magnitude constraints (Rohe et al., 2011; Sarkar and Bickel, 2015; Von Luxburg, 2007b), and also for product graphs such as the grid graph (shown in main text). Therefore, using eigenvectors upto λ_3 would suffice in these low rank cases even if the overall number of components was high.

16.10 Notes on the random walk augmentation in the SBM scenario

The random walk step in GCC (Qiu et al., 2020) is essential for the purposes of scaling Graph Contrastive methods. This is because in most cases, the ego-networks obtained by taking the simple neighbours within d steps of a node v are too large (over 1000) whereas a random walk on these ego networks, and then collecting the nodes visited, yields much smaller graphs (≤ 256 for our implementation, with averages much lower, < 100). This naturally leads us to ask if this step is only required for scalability - does it also have other desirable properties ?

In the stochastic block model, at least, it does. Consider the adjacency matrix of a 2-component SBM as A , with N nodes each of two classes. Let a node be v , and keep inter-connection probabilities as p, q, z .

For any p, q, z which are not arbitrarily low, i.e. do not $\rightarrow 0$ as $N \rightarrow 1$, it can be seen that any k -ego network of v for $k \geq 2$ covers a fraction of nodes $\rightarrow 1$ of the entire SBM. This can be understood by considering any node $v' \neq v$. There will be no path $v' \rightarrow z \rightarrow v$ (and in the other direction - we are dealing with undirected graphs) with $z \neq v, v'$ iff $\forall z$ there is either no edge (z, v) or no edge (z, v') .

The probability of such a path existing for a particular z is $\geq p_{min} = \min\{p^2, q^2, z^2, pz, qz, pq\}$. Therefore, any z will not have such a path with a probability $\leq 1 - p_{min}$. And, since there are $O(N)$ independent choices of z , such a path will **not**

exist between v, v' through such a z with a probability $\prod_{i=1}^{O(N)} (1 - p_{min})$. Thus, with probability $\rightarrow 1$ as $N \rightarrow \infty$, all such v, v' have a path between them of length 2. This implies all but 1-ego networks are unsuitable as they will include such paths and cover almost the entire graph.

The probability of a random walk, on the other hand, should be analyzed as follows. While it is tempting to consider the transition matrix (the adjacency matrix normalized by degree) for analysis and take its limit (as it enjoys well-understood properties), the random walks utilized in practice have a very high return probability to the origin (0.8). This implies, in turn, that we should only consider the random walk lengths of low step number, as the probability of visiting a node even at distance 3 is $0.2 \times 0.2 = 0.04$. Over a typical random walk of transition length 256, only 10 nodes at distance ≥ 3 occur.

With this in mind, consider a random walk starting WLOG from a node of class 0. Now :

- At walk length 1, the random walk has as neighbours, on expectation, $p(N - 1)$ nodes of class 0 and zN nodes of class 1.
- At the beginning of walk step 2, there is a roughly $\approx \frac{p}{p+z}$ probability the random walk is at label 0, and $\frac{z}{p+z}$ that it is at label 1. The corresponding probabilities at the end are : $\frac{p^2}{(p+z)^2} + \frac{z^2}{(z+q)(p+z)}$ for class 0 and $\frac{zq}{(z+q)(p+z)} + \frac{pz}{(p+z)^2}$ for class 1.

Compared to blindly taking the 2-ego network, this can be seen to notably bias the the network in favor of the first class, by a ratio equal to :

$$\frac{p^2(z+q) + z^2(p+z)}{zq(p+z) + pz(z+q)} = \frac{p^2z + p^2q + z^2p + z^3}{pqz + z^2q + pz^2 + pqz}$$

To see the numerator is greater, observe that $p^2z + z^3 \geq 2pz^2 \geq pz^2 + qz^2$ (AM-GM). This leaves us with proving that $p^2q + z^2p \geq 2pqz$. However, $p^2q + z^2p \geq pq^2 + z^2p \geq 2pqz$ (AM-GM). Therefore, unlike the 2-ego network case which virtually has the same number of nodes of either class with high probability, the random walk slants the node label ratio, as desired, in the 2-nd step (it trivially does so in the first step simply due to the 1-ego network case and this case has no interesting differences between the random walk and directly taking the ego network).

Ergo, the random walk may help offset nonsense nodes included in the ego-network, at least in the block model setting. The fact it is run with a high return probability aids this - were it allowed to run longer, it would approach its mixing time and be closer to uniform in its probability of being found over nodes of either class.

16.11 Larger ego networks

In this section, we have implicitly considered 1-ego networks when taking the full ego network into consideration. It is clear from our analysis in the random walk section that 2-ego networks or higher can only become feasible as at least one of p, q, z go to zero as N goes to infinity. Clearly, we cannot have z remain finitely large while p, q go to zero (as this violates our assumptions) and so either :

- all of p, q, z go to zero
- p, q stay finite, and z goes to zero.

Case 1 is much harder to tackle. For instance, our argument re : the Frobenius deviation in the adjacency matrix assumes that the expected adjacency matrix has a Frobenius norm of order $O(N^2)$. This may not be true when p, q, z are allowed to be infinitely small.

Instead, let p, q remain finite and $z \rightarrow 0$ as $N \rightarrow \infty$. Assume that the graph remains connected with high probability. This is true when, for instance, $z = 1/N$. The number of edges on expectation cross cluster is still $O(N)$. Observe that the crop proof we have used continues to work assuming no numerical problems. This is because the eigenvalues use $p + zc$, and c inversely varies as z . There are no infinities incurred as a result of z except for c itself. The value of $c \rightarrow \infty$, implying that post-normalization of eigenvectors, the cluster of label 0 receives embeddings which approach $[0, 0]$, and the cluster of label 1 receives embeddings which approach $[1, -1]$. The result also thus carries over to the similar embedding proof, which re-uses the crop result. In this particular case, 2 and higher ego networks are viable, and depend on the value of z . For

example, if $z = O(1/N)$, each node v in the cluster of label 0 has $O(1)$ neighbours in cluster 2, and $qN * O(1)$ neighbours at distance 2 of label 1, allowing 2-ego networks (3-ego networks fail in this case). We did not analyze such scenarios in depth, but we put the k_{max} in our theorem to allow such cases.

17 Time complexity analysis

First, we present the ego graph sizes as a function of average degree of the graphs and also as functions of the overall graph size. Then, we try to plot the time taken to process each graph instance as a function of these parameters.

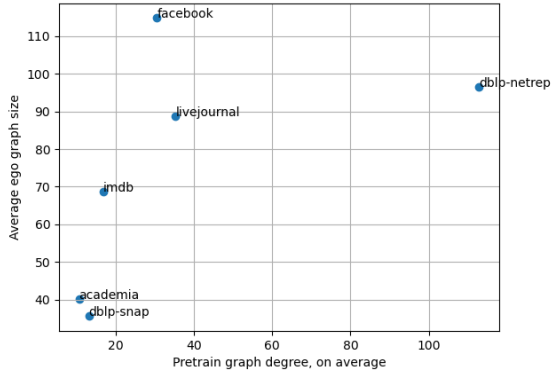


Figure 2: Average ego graph size vs pretrain graph degree.

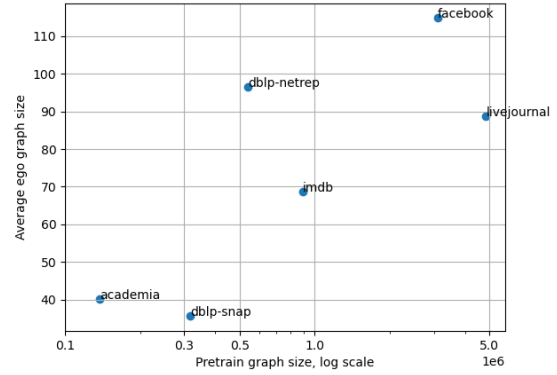


Figure 3: Ego graph size vs graph size

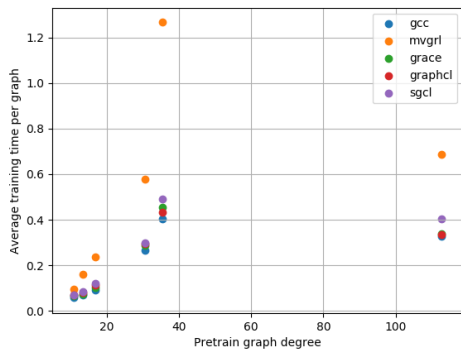


Figure 4: Time per graph vs average degree

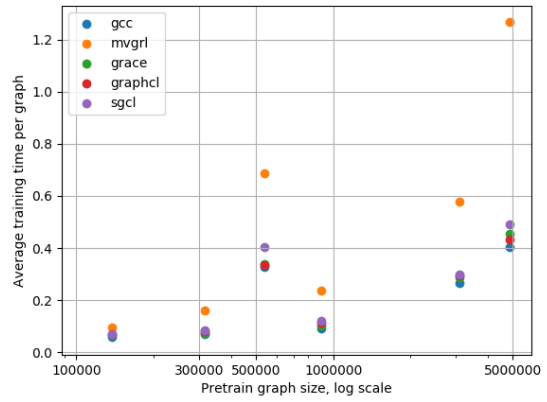


Figure 5: Time per graph vs graph size

18 Negative transfer effects

In some of our datasets, there is a noted **negative transfer effect**. What we mean by this is that further training actually decreases the performance on the dataset. One should be wary of this when looking at result pairs where, for instance, the pre-trained model performs worse than a non pre-trained model or a fresh model.

We repeat that the goal of pre-training is to come up with a general model that is trying to excel at all tasks, simultaneously - it is optimizing an average over all tasks. Optimizing such an average may come at the cost of a particular task. We illustrate this effect with IMDB-BINARY. We show 3 consecutive results on this dataset, E2E Frozen, at 5, 10, 20 epochs of training on DBLP. The results actually progressively worsen.

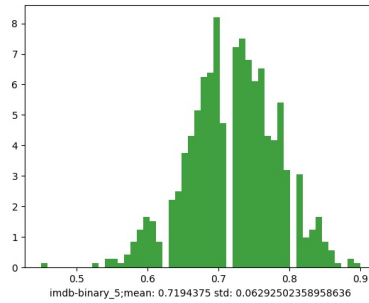


Figure 6: Performance on IMDB-Binary, 5 epochs

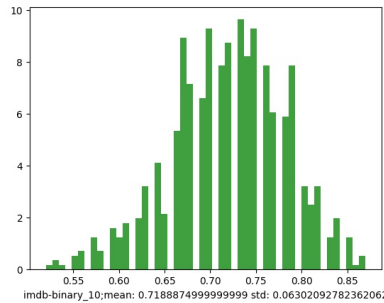


Figure 7: Performance on IMDB-Binary, 10 epochs

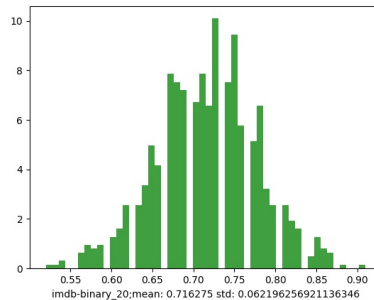


Figure 8: Performance on IMDB-Binary, 20 epochs

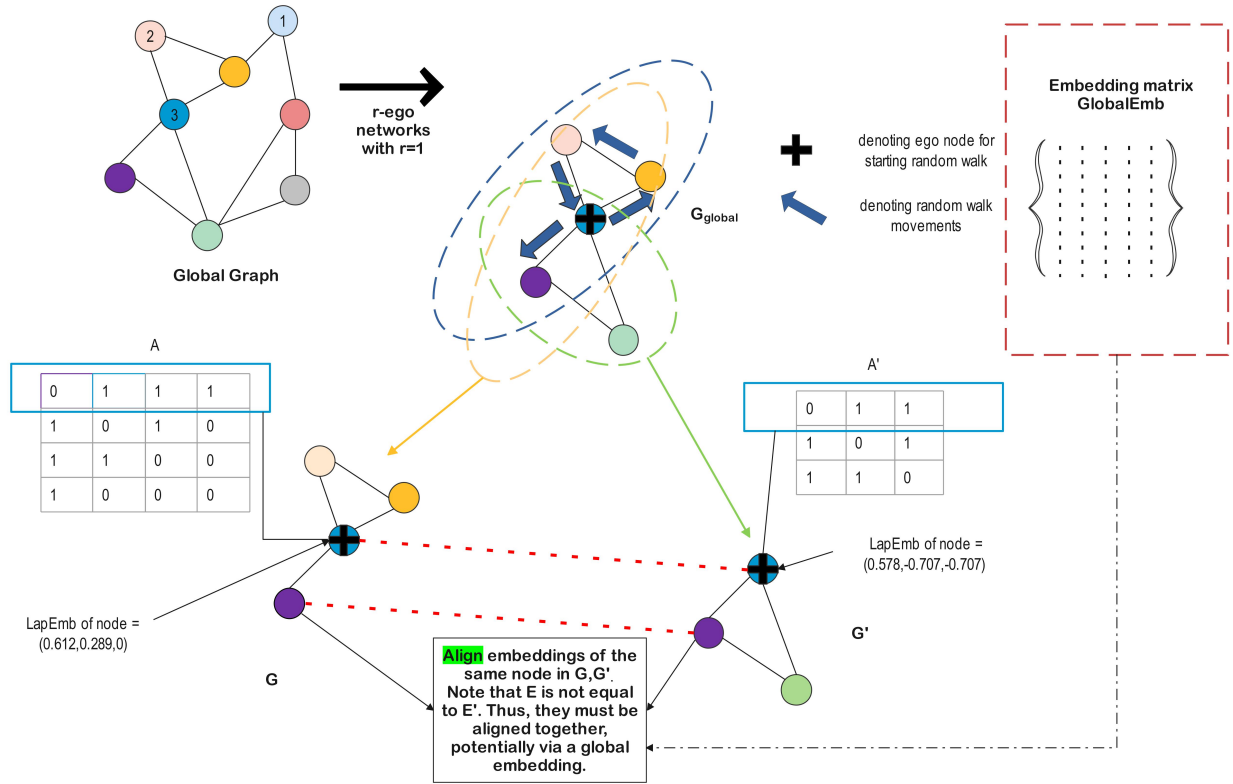


Figure 9: Alignment process overall

19 Visualizations of need for alignment

Here, we provide two illustrative figures 9, 10 we make that respectively demonstrate:

- The case where the global graph, after a random walk, can yield two views, which after Laplacian eigendecomposition end up with inconsistent embeddings for the same node, and thus requires alignment.
- The Wasserstein-Procrustes alignment process which is used as a subprocess to correct the inconsistent embeddings. Representative papers that explain the Wasserstein Procrustes method include CONE-ALIGN (Chen et al., 2020c)- especially in figures 1 and 2 and section 4.2 of the main text of the CONE-ALIGN paper, as well as REGAL (Heimann et al., 2018) and G-CREWE (Qin et al., 2020).

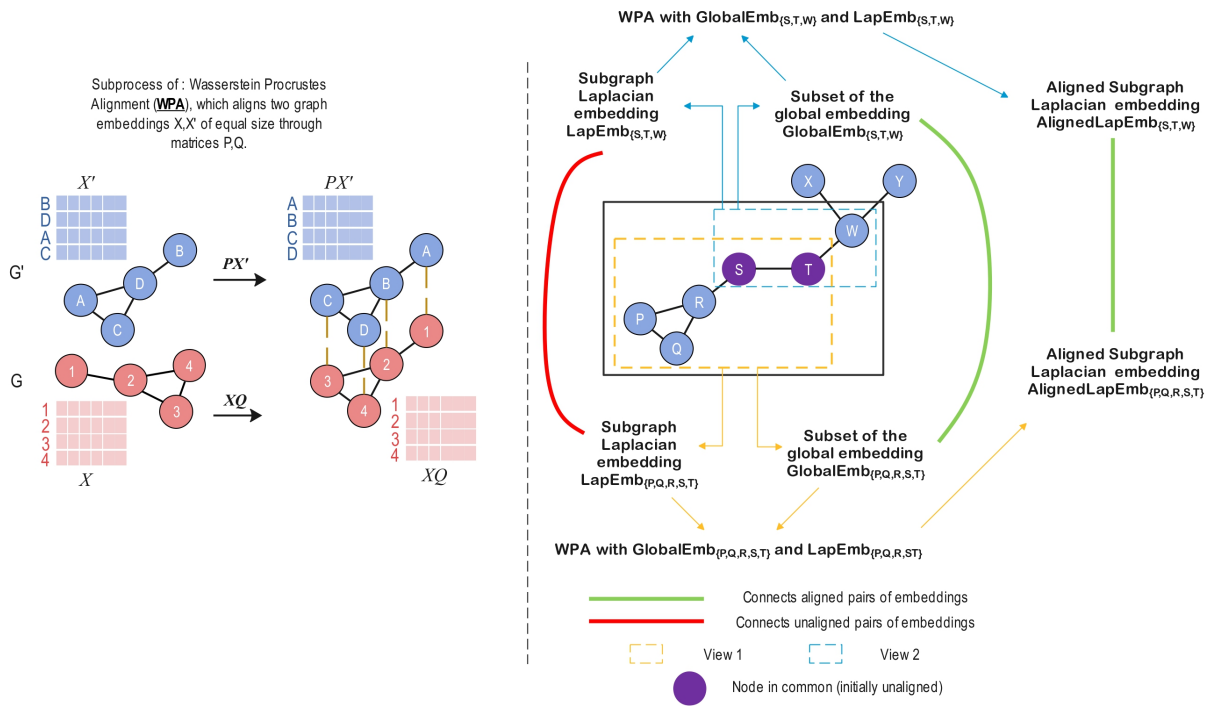


Figure 10: Alignment process detailed, with subprocess